To appear in
Computer Methods in Applied Mechanics and Engineering

Isogeometric shape optimization of photonic crystals via Coons patches

Xiaoping Qian

Department of Mechanical, Materials
and Aerospace Engineering
Illinois Institute of Technology
Chicago, IL 60062, USA
Email: qian@iit.edu

Ole Sigmund

Department of Mechanical Engineering
Technical University of Denmark
DK-2800 Kgs. Lyngby, Denmark
Email: sigmund@mek.dtu.dk

Abstract

In this paper, we present an approach that extends isogeometric shape optimization from optimization of rectangular-like NURBS patches to the optimization of topologically complex geometries. We have successfully applied this approach in designing photonic crystals where complex geometries have been optimized to maximize the band gaps.

Salient features of this approach include the following: 1) Multi-patch Coons representation of design geometry. The design geometry is represented as a collection of Coons patches where the four boundaries of each patch are represented as NURBS curves. The use of multiple patches is motivated by the need for representing topologically complex geometries. The Coons patches are used as a design representation so that designers do not need to specify interior control points and they provide a mechanism to compute analytical sensitivities for internal nodes in shape optimization. 2) Exact boundary conversion to the analysis geometry with guaranteed mesh injectivity. The analysis geometry is a collection of NURBS patches that are converted from the multi-patch Coons representation with geometric exactness in patch boundaries. The internal NURBS control points are embedded in the parametric domain of the Coons patches with a built-in mesh rectifier to ensure the injectivity of the resulting B-spline geometry, i.e. every point in the physical domain is mapped to one point in the parametric domain. 3) Analytical sensitivities. Sensitivities of objective functions and constraints with respect to design variables are derived through nodal sensitivities. The nodal sensitivities for the boundary control points are directly determined by the design parameters and those for internal nodes are obtained via the corresponding Coons patches.

Keywords: Shape optimal design, Isogeometric analysis, Photonic crystals, band gap

1 Introduction

This paper presents an isogeometric shape optimization approach that is applicable to topologically complex geometries.

Isogeometric shape optimization refers to the use of the same basis for both shape parameterization and analysis during the optimization. In the context of this paper, non-uniform rational B-spline (NURBS) is used for both shape parameterization and analysis. NURBS-based isogeometric shape optimization has several advantages over traditional shape optimization methods, including 1) Efficient shape parameterization. With a few control points, NURBS can represent complex freeform shape [1, 2]. 2) Computational advantage. The use of NURBS base in analysis has exhibited superior numerical properties, e.g. in terms of per-degree-of-freedom accuracy [3, 4] over traditional finite element analysis. 3) CAD compatibility. the output of NURBS-based shape optimization can be directly exported to a computer-aided design (CAD) system since the NURBS is the standard shape representation underlying all major CAD software.

Isogeometric shape optimization has recently been successfully applied in structural problems [5, 6, 7, 8, 9, 10]. However, the optimization of topologically complex geometry remains a challenge since the native NURBS representation is limited to rectangular-like shape due to its tensor-product nature. Recently, an approach based on trimmed spline surfaces [11, 12] has been proposed to address this issue.

In this paper, we present a multi-patch approach to the optimization of topologically complex geometries and apply this general concept to the maximization of band gaps (a range of frequencies in which the electromagnetic waves cannot propagate through a medium) in photonic crystals [13, 14]. The use of multiple NURBS patches is a natural choice for modeling complex models in isogeometric analysis as suggested in [3]. However, how to effectively create numerous (internal) NURBS control points in complex geometries and how to relate them to boundary shapes for sensitivity analysis in shape optimization remain unsolved. In this paper, the topological complexity is resolved via multiple compatible Coons patches which are then automatically converted into NURBS patches for analysis. Salient features of this approach include the following:

- Multi-patch Coons representation of design geometry. The design geometry is represented as a collection of Coons patches where the four boundaries of each patch are represented as NURBS curves. The use of multiple patches is motivated by the need for representing topologically complex geometries. The Coons patches are used as a design representation so that designers do not need to specify interior control points and they provide a mechanism to compute analytical sensitivities for internal nodes in shape optimization.

- Exact boundary conversion to the analysis geometry with guaranteed mesh injectivity. The analysis geometry is a collection of NURBS patches that are automatically converted from the multi-patch Coons representation. Each NURBS patch is converted from one Coons patch with geometrically identical patch boundary, although internal parameterization of Coons and NURBS patches may differ. The internal NURBS control points are embedded in the parametric domain of the Coons patches with a built-in mesh rectifier to ensure the injectivity of the resulting B-spline geometry, i.e. every point in the physical domain is mapped to one point in the parametric domain. It varies the position of internal NURBS control points until the minimal Jacobian of the geometry is positive.

- Analytical sensitivities. Sensitivities of objective functions and constraints with respect to design variables are derived through nodal sensitivities (i.e. the sensitivities of NURBS control points with respect to design variables). The nodal sensitivities for the boundary control points are directly determined by the design parameters. The sensitivities for internal nodes are obtained via the corresponding Coons patches since the internal control points of the NURBS patches are embedded in the parametric space of the Coons patches.

Although mesh creation via Coons patches, a form of transfinite interpolation, is a common algebraic approach for creating structured meshes in finite element analysis and shape optimization [15, 16], our approach differs from others in that the Coons surfaces themselves are not directly used as a mesh. Rather, Coons surfaces provide only a medium to generate (internal) control points for constructing the NURBS mesh for analysis. The method we use to rectify potentially invalid B-spline meshes is applicable to C^0 surfaces. It is done through explicit representation of the Jacobian of a B-spline surface as a higher-degree B-spline surface. The actual computation of the Jacobian is performed through its conversion to Bézier patches since they can provide a tighter bound than B-spline patches. We formulate this as a min-max optimization problem: maximizing the minimum of the Jacobian B-spline surface's control points until it becomes positive. We have successfully applied this shape optimization approach to the optimization of periodic cell shapes in photonic crystals for maximizing band gaps.

In the remainder of this paper, Section 2 describes how multiple compatible Coons patches can be constructed, how NURBS meshes for analysis can be constructed from the multiple Coons patches and how nodal sensitivities can be computed. In Section 3, we detail the procedure for ensuring that the B-spline mesh is valid (i.e. with positive Jacobian) for analysis. We present our shape optimization on topologically complex geometries in the context of maximizing band gaps in photonic crystals in Section 4. We conclude this paper in Section 5.

2 Constructing NURBS meshes via multiple compatible Coons patches

In this section, we first give basic definitions of curves and surfaces that are used in constructing multiple compatible Coons patches. We then show how NURBS meshes can be constructed from these multiple Coons patches.

2.1 Coons surface

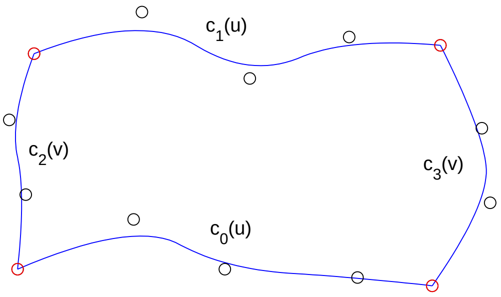

Figure 1: A Coons surface interpolates four NURBS boundary curves

A Coons surface interpolates two pairs of boundary curves $\boldsymbol{c}_0(u_0)$ and $\boldsymbol{c}_1(u_1)$, and $\boldsymbol{c}_2(v_0)$ and $\boldsymbol{c}_3(v_1)$. These four curves meet at four corners $\mathbf{S}(0,0)$, $\mathbf{S}(0,1)$, $\mathbf{S}(1,0)$, and $\mathbf{S}(1,1)$. A linearly blended Coons surface can be represented as

$$\begin{aligned}\mathbf{S}^c(u,v) \quad = \quad & (1-v)\boldsymbol{c}_0(u) + v\boldsymbol{c}_1(u) \\ & +(1-u)\boldsymbol{c}_2(v) + u\boldsymbol{c}_3(v) \\ & -(1-u)(1-v)\mathbf{S}_{00} - (1-u)v\mathbf{S}_{01} \\ & -u(1-v)\mathbf{S}_{10} - \mathbf{S}_{11}\end{aligned} \tag{1}$$

The boundary curves of a Coons patch are represented in NURBS. A degree p NURBS curve with $m+1$ control points $\mathbf{P}_i$ is represented as

$$\boldsymbol{c}(u) = \sum_{i=0}^{m} N_{i,p}\mathbf{P}_i \tag{2}$$

where $N_{i,p}$ is the p-th degree blending functions. When all the weights w_i are equal to one, the NURBS becomes a B-spline. In this paper, we are only concerned with B-splines. The use of rational B-spline in shape optimization is dealt with in [8]. An example of a Coons surface and the control points for defining its four boundary curves are shown in Fig. 1.

A Coons surface can be readily converted into a NURBS surface provided that the four boundary curves are compatible, that is 1) they share four corners; 2) each pair of boundary curves ($\boldsymbol{c}_0(u)$ and $\boldsymbol{c}_1(u)$ in u, $\boldsymbol{c}_2(v)$ and $\boldsymbol{c}_3(v)$ in v) have the same degree, knot vectors, and the number of control points. When the degrees and knots are not compatible, the compatibility can be achieved through knot insertion and degree elevation [17].

2.2 Constructing multi-patch Coons geometry

The multi-patch Coons geometry is a collection of Coons patches where the overlapping boundary between adjacent Coons patches have the same geometry and compatible representation. More specifically, the adjacent Coons patches are compatible in the sense 1) they are geometrically the same, 2) representation-wise, the overlapping portions of the two curves have the same degree and same control points, and 3) the end points of the overlapping curves are C^0 end points. The goal of such compatibility requirement is to ensure that adjacent patches, upon mesh refinement, remain geometrically and parametrically the same. Note, however, that the knot vectors are allowed to be scaled and offset to make them compatible.

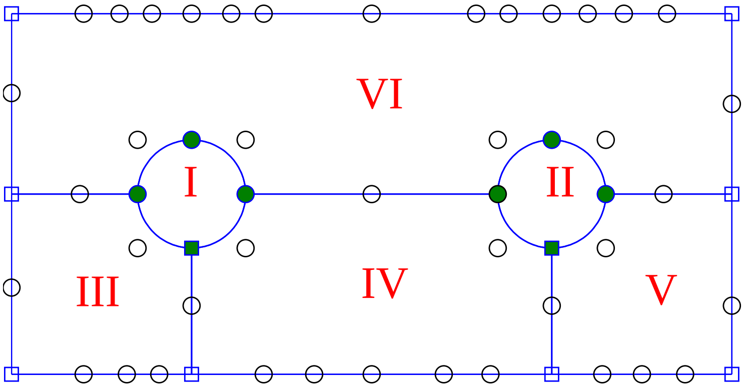

Figure 2: Multiple compatible Coons patches. Corner points in Patch I and II are shown as filled markers. Corners points in Patch III, IV, V, and VI are shown as square markers.

Fig. 2 shows a multi-patch representation of a plate with two circular inclusions. It is composed of six bi-quadratic Coons patches. All the boundary curves are represented in NURBS. This example illustrates different scenarios of overlapping among adjacent patches: 1) Patch I overlaps with patch III and patch IV by quarter circles. It also overlaps with patch VI by a half circle. 2) The top part of the plate is made of one patch (VI) and the bottom part is made of three patches (III, IV, V), although the shape is symmetrical. This illustrates the flexibility of multi-patch modeling in that the same shape can be represented in different ways. 3) All overlapping boundaries between adjacent patches have exactly the same shape. These overlapping curves are also parametrically the same when knots are scaled and offset accordingly. Therefore, when the patches are refined for analysis, the overlapping boundary curves remain geometrically and parametrically the same.

Each Coons patch will be converted to one single NURBS patch. This one-to-one mapping is always maintained. The number of Coons patches depends on the number of boundary curves in the design geometry and the shape and topology of the design geometry. How to automatically generate Coons patches is a task yet to be automated. In general, the number of Coons patches is never more than the number of boundary curves. Each Coons patch is created to be as rectangular as possible with its boundary being conformal to the boundary shape.

2.3 Creating the NURBS analysis model

A NURBS surface is represented as

$$\mathbf{S}(u,v)=\frac{\displaystyle\sum_{i=0}^{m}\sum_{j=0}^{n}N_{i,p}N_{j,q}w_{i,j}\mathbf{P}_{ij}}{\displaystyle\sum_{i=0}^{m}\sum_{j=0}^{n}N_{i,p}N_{j,q}w_{ij}} \tag{3}$$

where $N_{i,p}$ and $N_{j,q}$ are p-th and q-th degree B-spline functions, w_{ij} and $\mathbf{P}_{ij}$ are ij-th weight and control point for the NURBS surface, respectively.

An array of $(m+1)\times(n+1)$ control points are needed to define a NURBS surface. Each Coons patch corresponds to one single NURBS patch. When converted from a Coons patch defined with four compatible boundary curves, these boundary curves' control points become the boundary control points of the NURBS curves. Only the internal $(m-1)\times(n-1)$ control points need to be additionally generated for completely defining a NURBS surface. Note that, for reasons to be described in the subsection below, each Coons patch and the converted NURBS patch only share the same patch boundary and the internal parameterizations may be different. For example, Fig. 3 shows a NURBS surface converted from the Coons patch in Fig. 1 where the boundary control points of the NURBS come from the Coons patch and the internal control points that need to be generated are marked in red. We show below how internal control points are generated.

2.3.1 Creating initial internal control points

The internal control points are generated in such a way that their sensitivities with respect to the boundary shape changes as parameterized by design variables can be easily obtained. Therefore, we embed the NURBS surface's internal control points on the parametric domain of the Coons patch. That is,

$$\mathbf{P}_{ij}=\mathbf{S}^{c}(\widetilde{u}_i,\widetilde{v}_j),\quad i=1,\cdots,m-1,\ j=1,\cdots,n-1. \tag{4}$$

One method to specify the parametric coordinates of the internal control points is based on

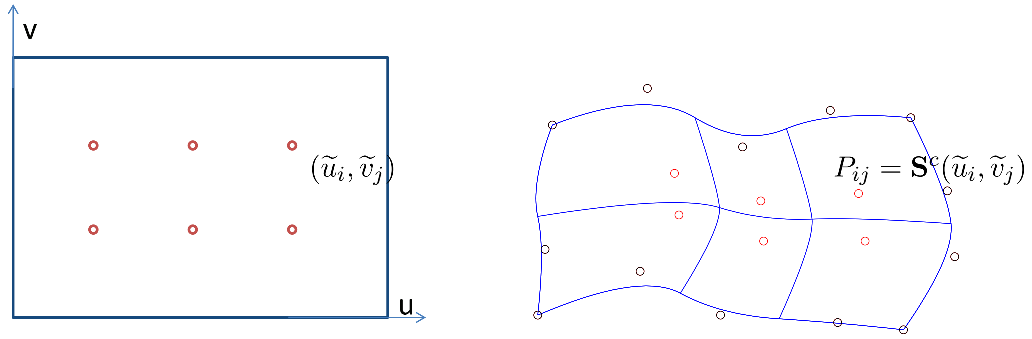
v
u
$(\widetilde{u}_i, \widetilde{v}_j)$
$P_{ij} = \mathbf{S}^c(\widetilde{u}_i, \widetilde{v}_j)$

(a) The uv domain of a Coons patch

(b) NURBS patch and internal control points

Figure 3: NURBS surface constructed from the Coons patch in Fig. 1

their order in the sequence of boundary control points. That is,

$$\widetilde{u}_i = \frac{i}{m}, \qquad \widetilde{v}_j = \frac{j}{n} \tag{5}$$

This method is effective when the control points are placed approximately equidistantly, leading to approximately same element size, both geometrically and parametrically. In this paper, all results shown are generated based on Eq. (5).

Fig. 3 shows the internal NURBS control points defined in the parametric domain of a Coons patch. Fig. 4 shows the internal control points generated from multiple Coons patches shown in Fig. 2 with this method. The knot curves are displayed in blue and the internal control points are displayed in red. The resulting knots curves demarcate the element boundary for isogeometric analysis.

An alternative would be to link the parametric separation of control points with their physical separation of boundary control points as follows. If we assume the first curve's control points $P^1_0, P^1_1, \cdots, P^1_m$, and the second curve's control points $P^2_0, P^2_1, \cdots, P^2_m$, we can set

$$\widetilde{u}_i = \frac{1}{2}\left(\frac{\sum_{k=0}^{i} ||P^1_{i-1}P^1_i||}{\sum_{k=0}^{m-1} ||P^1_k P^1_{k+1}||} + \frac{\sum_{k=0}^{i} ||P^2_{i-1}P^2_i||}{\sum_{k=0}^{m-1} ||P^2_k P^2_{k+1}||}\right), \quad i = 1, \cdots, m-1$$

The $\widetilde{v}_j$ coordinates can be created likewise from the third and fourth boundary curves.

Another alternative would be to convert Coons patches exactly into NURBS patches. The process however is cumbersome since it would require degree elevations for bilinear surfaces interpolating the four corner points and degrees matching between the two ruled surfaces interpolating the two pairs of boundary curves.

All methods can lead to reasonably good NURBS meshes, but none of them guarantees that the generated meshes are always valid. Fig. 5 shows, based on (5), that a slight change of one boundary control point in the example shown in Fig. 4 would lead to an invalid NURBS mesh in the sense that there is fold-over, i.e. two points in the parametric domain of the NURBS surface would be mapped to the same physical point. To preclude this problem, a method for rectifying the initial mesh is suggested in Section 3. In this rectification, a new $(\widetilde{u}, \widetilde{v})$ is found for each internal control point so that the resulting NURBS mesh is valid.

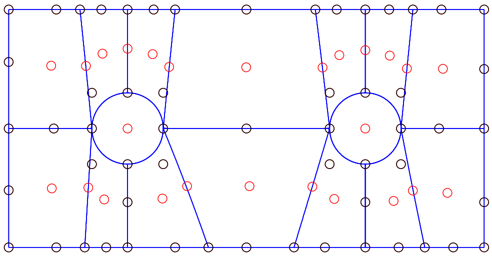

Figure 4: Multiple compatible NURBS patches created from multiple Coons patches by adding internal control points

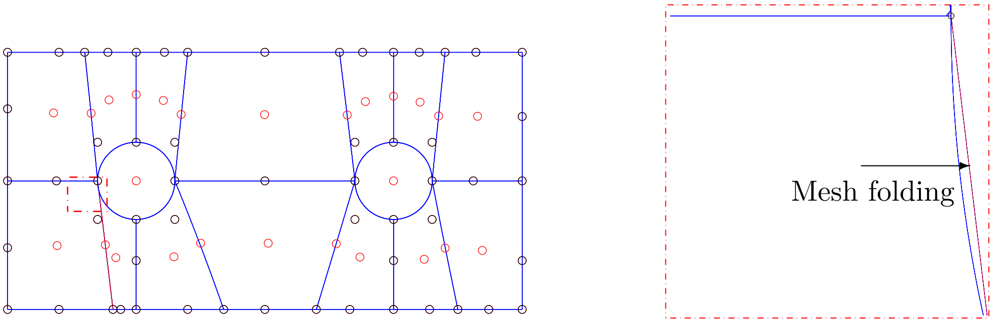

(a) Original mesh

(b) Magnified view

Figure 5: Creating NURBS internal control points directly from Coons may lead to mesh fold-over.

2.3.2 Refining the analysis model

The NURBS model constructed from multiple Coons patches, upon rectification when necessary, may not have sufficiently dense elements for the accurate analysis required by shape optimization. The NURBS analysis model can thus be obtained through mesh refinement [8]. A knot insertion algorithm for creating quasi-uniform mesh in the physical space is available in [3]. In addition, p-refinement and k-refinement methods are described in [18]. In the section below, we briefly present the basic procedure for h-refinement through knot insertion.

Knot insertion refers to adding a new knot into the existing knot vector without changing the shape of the curve. Because the fundamental equality for a B-spline curve is that $m = n + p + 1$ where $m + 1$ is the total number of knots for a degree p B-spline curve with $n + 1$ control points, inserting a new knot requires a new control point to be added. (More precisely), some existing control points are removed and new ones are added.

Given a set of $n+1$ control points $P_0, P_1, ..., P_n$, a knot vector $\{\xi_0, \xi_1, ..., \xi_m\}$ and a degree p, we can insert a new knot $\bar{\xi}$ into the knot vector without changing the shape of the B-spline curve $\boldsymbol{x}(\xi)$ as follows. Assuming we need to insert a knot $\bar{\xi}$ into the knot span $[\xi_l, \xi_{l+1}]$, we have the following basic knot insertion procedure for a B-spline curve:

- Find l such that $\bar{\xi}$ lies in the knot span $[\xi_l, \xi_{l+1}]$.
- Find $p + 1$ control points $P_{l-p}, P_{l-p+1}, ..., P_l$.
- Compute p new control points Q_i from the above $p + 1$ control points by using the formula

$$Q_i = (1 - \beta_i)P_{i-1} + \beta_i P_i, \tag{6}$$

where the ratio β_i is computed as below:

$$\beta_i = \frac{\bar{\xi} - \xi_i}{\xi_{i+p} - \xi_i} \qquad \text{for } l - p + 1 \leq i \leq l.$$

The above process can be readily extended to a NURBS curve refinement and NURBS surface refinement [17]. Fig. 6.a shows the 6-patch Coons model and Fig. 6.b shows the refined NURBS mesh after knot insertion.

2.4 Computing nodal sensitivities

One of the key tasks in gradient-based shape optimization is to compute nodal sensitivities, i.e. computing how the mesh nodes (control points in the context of isogeometric analysis) change with respect to design variables $\boldsymbol{\alpha}$. Design variables $\boldsymbol{\alpha}$ control the boundary shape to be optimized. These design boundary curves as represented in (2) are a subset of the boundary curves of Coons patches (1). The internal control points of the NURBS surface (3) are defined in the Coons patch's parametric domain (5). When mesh refinement is desired, knot insertion is invoked as shown in (6). By differentiating these equations, (2), (1) , (5) , and (6) over the design variables, one can obtain the analytical nodal sensitivities. In practice, these sensitivities are obtained by directly differentiating these expressions (equations (2), (1), (5) and (6)). Such differentiation can be done analytically by hand or symbolically with an algebraic manipulation program (i.e. Mathematics or Maple). The results can then be inserted in the computer code.

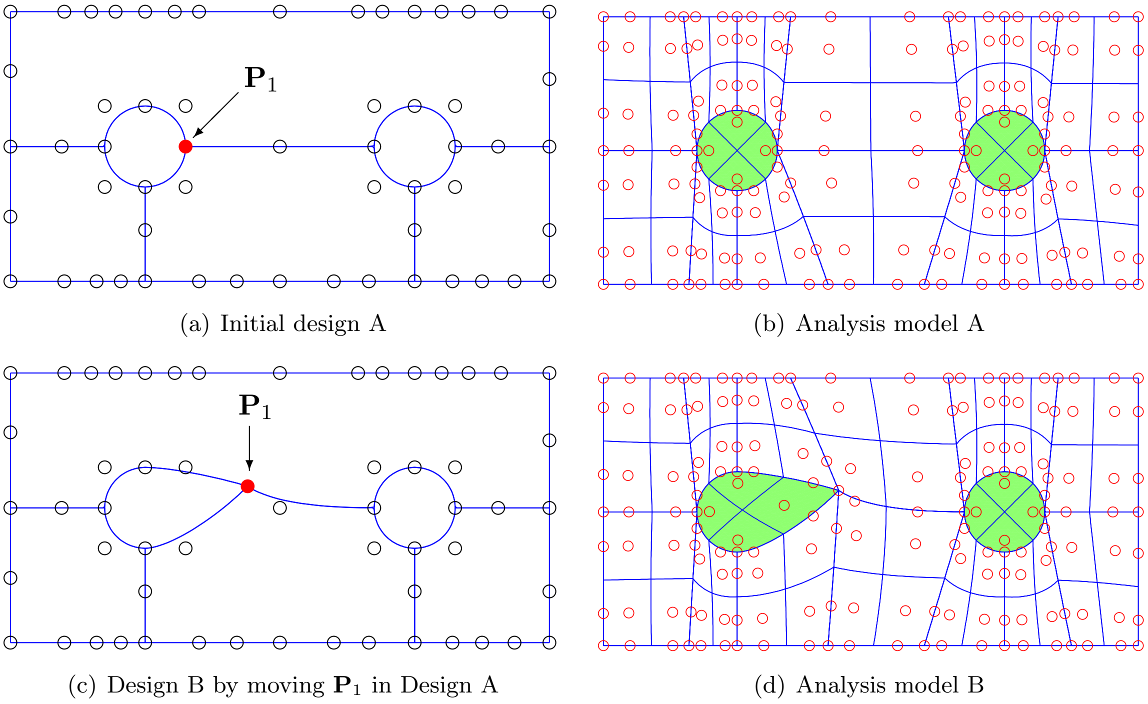

(a) Initial design A

(b) Analysis model A

(c) Design B by moving $\mathbf{P}_1$ in Design A

(d) Analysis model B

Figure 6: Nodal sensitivity propagating the influence of design variables to the analysis nodes

Fig. 6 gives an example where a 5-patch Coons design model is used to construct the NURBS analysis model. From the Coons patches (Fig. 6.a), its internal control points are first generated to construct a NURBS model (Fig. 4) and 1×1 (once in u and once in v directions) knot insertion is invoked to obtain the analyis model (Fig. 6.b). When the design variable $\mathbf{P}_1$ is moved (Fig. 6.c), the new nodal positions in the analysis model can then be regenerated according to the procedure described above. Sensitivity of each node in the analysis model with respect to $\mathbf{P}_1$ can be computed analytically by differentiating the above equations.

3 B-spline mesh rectification

The procedure described in the above section, although usually generating a good quality mesh, may lead to meshes with fold-over during optimization, i.e. two parametric points correspond to one spatial point. This is especially true when the boundary curves from the Coons patches contain C^0 points, which allows sharp kinks of the boundary curve. This mesh fold-over is caused by the changing sign of the Jacobian of the geometric mapping from the parametric domain to the physical space. Unless otherwise noted, in this paper, we assume the boundary of Coons patches is so constructed that it admits surface parameterization with positive Jacobian. When some portion of the surface has negative Jacobian, the fold-over occurs. An example is shown in Fig. 7, where the initial B-spline surface converted from the Coons patch is defined by a bi-quadratic 5×3 control net. The knot vectors are $U = \{0, 0, 0, 0.5, 0.5, 1, 1, 1\}$ and $V = \{0, 0, 0, 1, 1, 1\}$. The three internal control points are marked in red. The B-spline surface is subdivided many times to show the fold-over. The magnified view of the fold-over is shown in Fig. 7.b. The corrected B-spline mesh by varying the internal control points in the parametric domain (Fig. 7c) are shown in Fig. 7d.

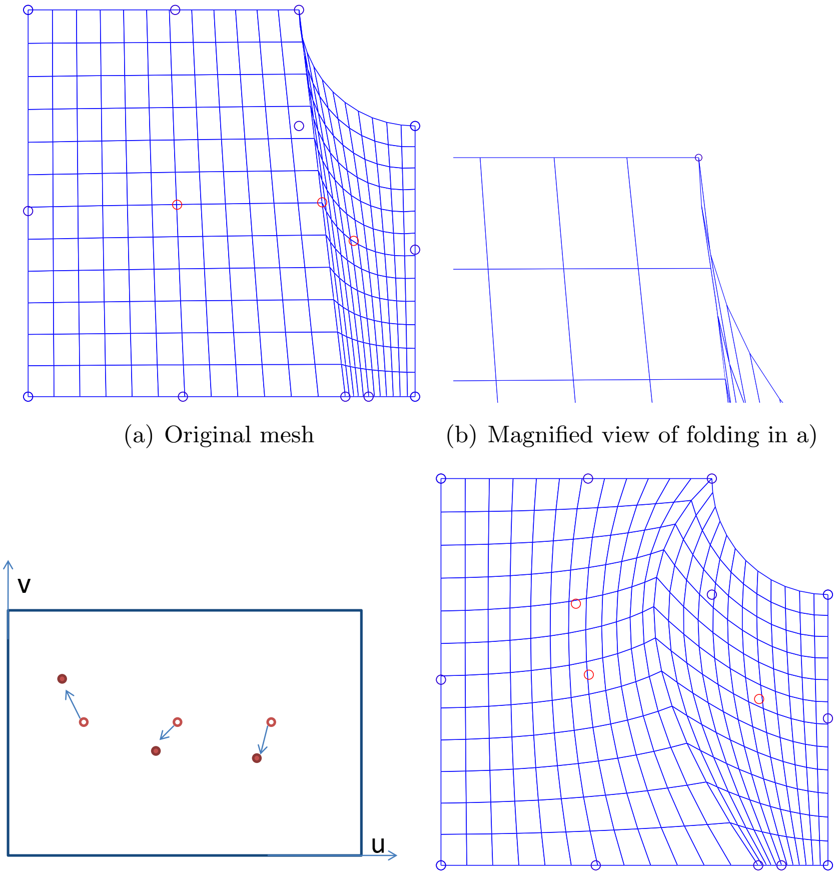

(a) Original mesh

(b) Magnified view of folding in a)

(c) Varying control point positions in the uv domain of the Coons patch

(d) Rectified mesh

Figure 7: Rectifying a bad B-spline mesh by varying internal control points (red points)

Our B-spline mesh rectification approach seeks to vary a B-spline surface $\mathbf{S}(u,v)$'s internal control points $\mathbf{P}_{ij}$ by changing their positions , $(\widetilde{u}_i, \widetilde{v}_j)$ (cf. Eqs. (4) and (5)), in the parametric domain of the Coons patch until the B-spline surface's Jacobian $J(u,v)$ is positive. The premise of this approach is that in order to ensure a B-spline surface's injectivity, the Jacobian of the B-spline surface needs to be positive. The basic approach to ensure the surface's injectivity is based on the fact that the Jacobian of a B-spline surface remains a B-spline surface (by forming the product of B-splines into a B-spline form [19]) and through a sufficient condition that, if all control points of the Jacobian B-spline surface is positive, then the Jacobian is positive.

Similar approaches to prevent self-intersection have been attempted in the past, including preventing self-intersection under free-form deformation [20], and generating non-self-overlapping quadrilateral grids from a Bézier patch [21]. In the context of isogeometric analysis, an effort to obtain optimal B-spline parameterization via Winslow functional with positive Jacobian as a constraint is also being conducted [9]. However, our approach is applicable to C^0 B-spline surfaces without an extra layer of phantom zone [20] or repeated control vertices [22].

Our assumption is that the boundary control points of the B-spline surface allows such a valid B-spline mesh. In order to obtain a tighter bound on the Jacobian, our approach subdivides the original B-spline surface, converts the subdivided surface into Bézier patches, computes the Jacobian of the Bézier patches and recomposes them into the B-spline form. We adopt a gradient-based optimization approach to maximize the minimal control point of the Jacobian B-spline surfaces until the minimal control point is positive. Since analytical gradients are used, the gradient-based optimization converges very fast to a positive Jacobian, typically in a few iterations.

We detail below our approach to rectifying the B-spline mesh.

3.1 Jacobian of a B-spline surface

We first show that the Jacobian of a B-spline surface is a higher degree B-spline surface.

Let the B-spline surface $\mathbf{S}(u,v)$ be represented as

$$\mathbf{S}(u,v) = \sum_{i=0}^{m}\sum_{j=0}^{n} N_{i,p}(u)N_{j,n}(v)\mathbf{P}_{ij} \tag{7}$$

The Jacobian is

$$J(u,v) = \det\begin{bmatrix}\mathbf{S}_u & \mathbf{S}_v\end{bmatrix}$$

$$\mathbf{S}_u(u,v) = \sum_{i=0}^{m-1}\sum_{j=0}^{n} N_{i,p-1}(u)N_{j,q}(v)\alpha_i(\mathbf{P}_{(i+1)j} - \mathbf{P}_{ij})$$

$$\mathbf{S}_v(u,v) = \sum_{k=0}^{m}\sum_{l=0}^{n-1} N_{k,p}(u)N_{l,q-1}(v)\beta_l(\mathbf{P}_{k(l+1)} - \mathbf{P}_{kl})$$

where

$$\alpha_i = \frac{p}{u_{p+i+1} - p_{i+1}}, \quad \beta_l = \frac{q}{v_{q+l+1} - v_{l+1}}$$

If we note $\Delta\mathbf{P}_{ij,u} = \mathbf{P}_{(i+1)j} - \mathbf{P}_{ij}$ and $\Delta\mathbf{P}_{kl,v} = \mathbf{P}_{k(l+1)} - \mathbf{P}_{kl}$, we have

$$J(u,v) = \sum_{i=0}^{m-1}\sum_{j=0}^{n}\sum_{k=0}^{m}\sum_{l=0}^{n-1} N_{i,p-1}(u)N_{j,q}(v)N_{k,p}(u)N_{l,q-1}(v)\alpha_i\beta_l \det\begin{bmatrix}\Delta\mathbf{P}_{ij,u} \; \Delta\mathbf{P}_{kl,v}\end{bmatrix} \tag{8}$$

Note, the product of two B-splines is a higher-degree B-spline, as first reported in [19].

$$N_{i,p}(t)N_{j,q}(t) = \sum_{h} \Gamma_{i,j,p,q,}(h)N_{k,p+q}(t)$$

where the coefficient $\Gamma_{i,j,p,q}(h)$ is recursively defined in [19]. The knot vectors for the new B-spline is a union of all knots in the two knot vectors of its component B-splines with the knot mulitiplicity as

$$m_i = \begin{cases} \max(p+m_a, q+m_b), & m_a > 0 \text{ and } m_b > 0 \\ p + m_b, & m_a = 0 \text{ and } m_b > 0 \\ q + m_a, & m_a > 0 \text{ and } m_b = 0 \end{cases} \tag{9}$$

where m_a represent the knot t_i's multiplicity in the B-spline a and m_b the knot multiplicity in B-spline b.

Thus the multiplication of four B-spline basis functions in Eq. (8), $N_{i,p-1}(u)N_{j,q}(v)N_{k,p}(u)N_{l,q-1}(v)$, leads to $\sum\limits_s \Gamma_s N_{s,2p-1}(u) \sum\limits_t \Gamma_t N_{t,2q-1}(v)$. By rearranging all the coefficients for $N_{s,2p-1}(u)N_{t,2q-1}(v)$, Eq. (8) becomes

$$J(u,v) = \sum_{s=0}^{2m-1} \sum_{t=0}^{2n-1} N_{s,2p-1}(u)N_{t,2q-1}(v)J_{st} \tag{10}$$

where J_{st} is the control point of the B-spline representation of the Jacobian of the original surface $\mathbf{S}(u,v)$ (7).

Eq. (10) thus shows that the Jacobian of a B-spline surface is itself a B-spline surface.

3.2 Jacobian of a Bézier patch

Since Bézier patches, when converted from a B-spline surface, have tighter convex hulls than that of the original B-spline surface, we do not directly compute $\mathbf{J}_{st}$ of a B-spline surface. Rather, we obtain the Jacobian surface via the Bézier patches. The Bézier patches are obtained by inserting the knots until the continuity at internal knots becomes C^0. Note, we can easily recompose the Jacobian B-spline surface from the Jacaobian of Bézier surfaces [23] since we know the knot multiciplity in u and v directions based on (9).

If we denote a Bézier surface patch $\mathbf{S}(u,v)$ as

$$\mathbf{S}(u,v) = \sum_{i=0}^{p} \sum_{j=0}^{q} B_{i,p}(u)B_{j,q}(v)\mathbf{P}_{ij}$$

The Jacobian is

$$J(u,v) = \det \begin{bmatrix} \mathbf{S}_u & \mathbf{S}_v \end{bmatrix}$$

$$\mathbf{S}_u(u,v) = \sum_{i=0}^{p-1} \sum_{j=0}^{q} B_{i,p-1}(u)B_{j,n}(v)p(\mathbf{P}_{(i+1)j} - \mathbf{P}_{ij})$$

$$\mathbf{S}_v(u,v) = \sum_{k=0}^{p} \sum_{l=0}^{q-1} B_{k,p}(u)B_{l,q-1}(v)q(\mathbf{P}_{k(l+1)} - \mathbf{P}_{kl})$$

If we denote $\Delta\mathbf{P}_{ij,u} = \mathbf{P}_{(i+1)j} - \mathbf{P}_{ij}$ and $\Delta\mathbf{P}_{kl,v} = \mathbf{P}_{k(l+1)} - \mathbf{P}_{kl}$, we have

$$J(u,v) = \sum_{i=0}^{p-1} \sum_{j=0}^{q} \sum_{k=0}^{p} \sum_{l=0}^{q-1} B_{i,p-1}(u)B_{j,q}(v)B_{k,p}(u)B_{l,q-1}(v)pq \det \begin{bmatrix} \Delta\mathbf{P}_{ij,u} & \Delta\mathbf{P}_{kl,v} \end{bmatrix} \tag{11}$$

Note, the product of Bernstein polynomials is a higher-degree Bernstein polynomial [24]

$$B_{i,p}(t)B_{j,q}(t) = \frac{\binom{p}{i}\binom{q}{j}}{\binom{p+q}{i+j}} B_{i+j,p+q}(t)$$

Eq. (11) then becomes

$$\begin{aligned} J(u,v) &= \sum_{i=0}^{p-1}\sum_{j=0}^{q}\sum_{k=0}^{p}\sum_{l=0}^{q-1} \frac{\binom{p-1}{i}\binom{p}{k}}{\binom{2p-1}{i+k}} B_{i+k,2p-1}(u) \frac{\binom{q}{j}\binom{q-1}{l}}{\binom{2q-1}{j+l}} B_{j+l,2q-1}(v) \\ &\qquad pq \det\left[\Delta\mathbf{P}_{ij,u}\ \Delta\mathbf{P}_{kl,v}\right] \qquad (12) \\ &= \sum_{s=0}^{2p-1}\sum_{t=0}^{2q-1} B_{s,2p-1}(u)B_{t,2q-1}(v)J_{st} \end{aligned}$$

where

$$J_{st} = \sum_{\substack{i+k=s,\\ i\in[0,p-1],\\ k\in[0,p]}} \sum_{\substack{j+l=t,\\ j\in[0,q],\\ l\in[0,q-1]}} pq \frac{\binom{p-1}{i}\binom{p}{k}}{\binom{2p-1}{i+k}} \frac{\binom{q}{j}\binom{q-1}{l}}{\binom{2q-1}{j+l}} \det\left[\Delta\mathbf{P}_{ij,u}\ \Delta\mathbf{P}_{kl,v}\right] \qquad (13)$$

It is thus clear from Eq. (12) that the Jacobian of a Bézier surface patch is a higher-degree Bézier surface.

3.3 Recomposing the Jacobian of a B-spline surface

After each Bézier patch's Jacobian is computed into a Bézier form (13), they can be recomposed into a B-spline form. This is needed since otherwise overlapping Bézier patches would lead to redundant constraints (i.e. Jacobian control points) for optimization. Here we retain the C^0 form of the Jacobian B-spline in order to keep the bound tight.

For a B-spline surface $\mathbf{S}$ of degree $p \times q$ that is at least C^1 continuous, we first subdivide it $a \times b$ times in order to obtain a tighter convex hull bound. If we assume there are n_{eu} Bézier segments in the u direction and n_{ev} Bézier segments in the v direction after $a \times b$ times of refinement of the surface $\mathbf{S}$, the Jacobian of the original B-spline surface $\mathbf{S}(u,v)$ is a B-spline surface of degree $(2p-1)\times(2q-1)$, consisting of $n_{eu} \times n_{ev}$ Bézier segments of degree $(2p-1)\times(2q-1)$, totaling $(n_{\text{eu}}(2p-1)+1)\times(n_{\text{ev}}(2q-1)+1)$ control points. We refer to these control points as the control points of the Jacobian B-spline surface.

However, if the B-spline surface $\mathbf{S}$ is C^0, we need to first decompose it into a collection of surfaces $\mathbf{S}^i$ that are at least C^1 continuous. The Jacobian is then computed separately for each $\mathbf{S}^i$. This is more advantageous than adding a layer of phantom zone [20] or repeating control vertices [22] since it does not involve any computing other than separating $\mathbf{S}$ into surfaces $\mathbf{S}^i$ that are at least C^1.

3.4 Maximizing the minimal Jacobian

If all the control points of the Jacobian B-spline surface are larger than 0, the B-spline surface $\mathbf{S}$ is invertible, i.e. we have successfully rectified the B-spline mesh. This leads to an optimization based formulation for obtaining an invertible B-spline surface.

The overall approach for rectifying a bad B-spline mesh with negative Jacobian is shown in Fig. 8. It can be summarized as follows

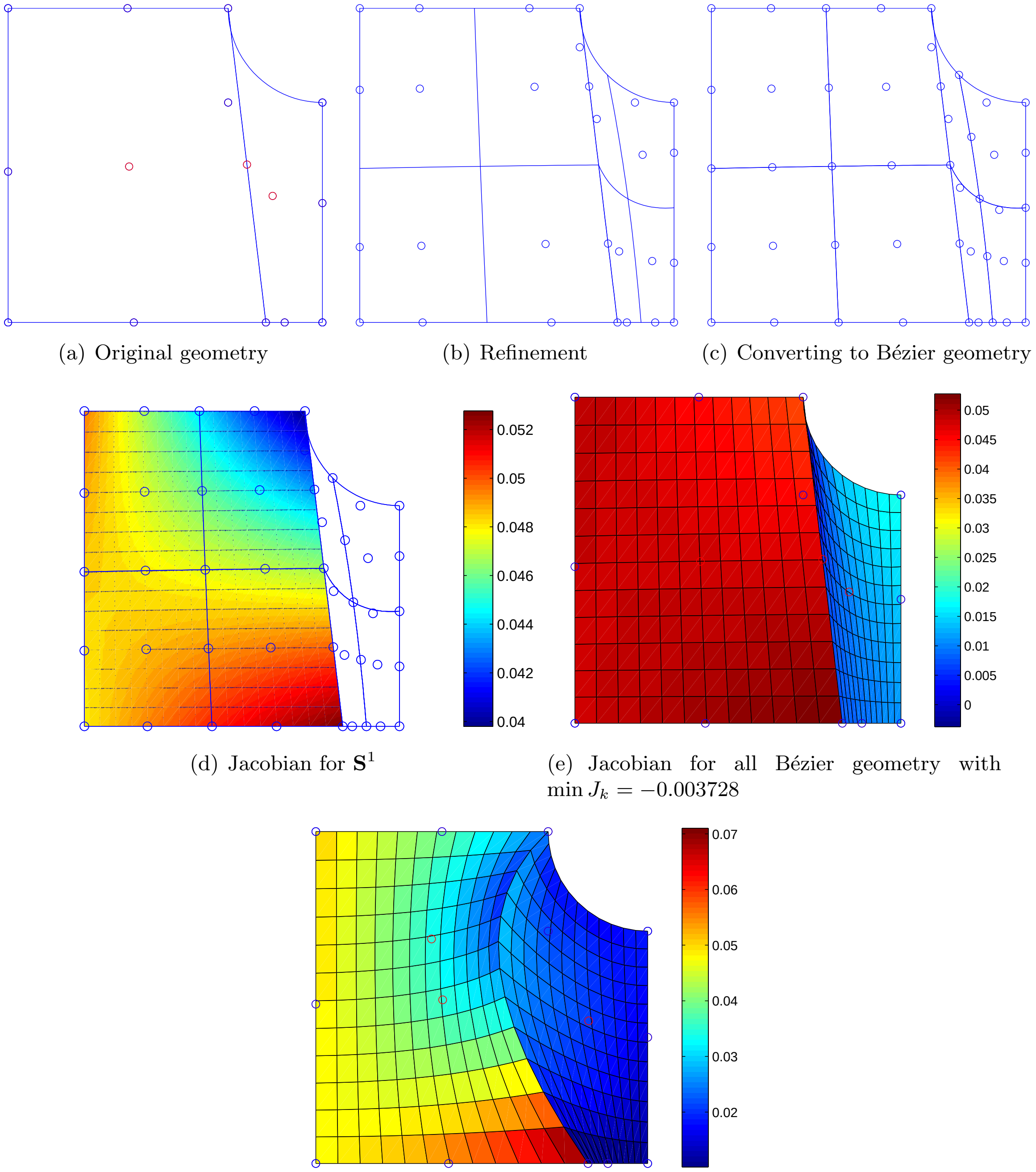

(a) Original geometry

(b) Refinement

(c) Converting to Bézier geometry

(d) Jacobian for $\mathbf{S}^1$

(e) Jacobian for all Bézier geometry with $\min J_k = -0.003728$

(f) Jacobian for corrected geometry with $\min J_k = 0.010145$

Figure 8: Procedure for rectifying a bad B-spline mesh by varying internal control points (red points). It only took one iteration.

- Separate B-spline surface $\mathbf{S}$ into a collection of B-spline surfaces each of which is at least C^1 continuous $\mathbf{S}_i$
- Subdivide each $\mathbf{S}^i$ $a \times b$ times and obtain $\widetilde{\mathbf{S}}^i$
- Knot insertion to extract all Bézier patches $\overline{\widetilde{\mathbf{S}}}^i$ from each subdivided surface $\widetilde{\mathbf{S}}^i$
- Compute Jacobian for each Bézier patch
- Recompose Jacobian for Bézier patches into C^0 Jacobian B-splines for each $\mathbf{S}^i$.
- Maximize the minimum Jacobian of all B-spline surfaces $\mathbf{S}^i$ until it is larger than zero.

To simplify the notation in optimization, we reformulate the double index of control points in B-spline surfaces into a single index. For example, we note the collection of internal control points' physical coordinates $\mathbf{P}_{ij} = \begin{bmatrix} x^1_{ij} & x^2_{ij} \end{bmatrix}$ as $\boldsymbol{\gamma}$ and the corresponding parameters in the parameter space of the Coons surface as $\boldsymbol{\gamma}^u$.

Equation (12) can now be rewritten as

$$\det \mathbf{S}^i = \sum_k N_k \overline{\widetilde{J}}^i{}_k(\boldsymbol{\gamma})$$

The convex hull property of the B-spline representation leads to

$$\min_k \overline{\widetilde{J}}^i{}_k \leq \min_{u,v} \det S^i(u, v)$$

Therefore, when

$$\min_{i,k} \overline{\widetilde{J}}^i{}_k(\boldsymbol{\gamma}) > 0 \tag{14}$$

we have a valid mesh.

Remark 1. The criterion (14) for determining if a mesh is valid is a sufficient (i.e. conservative) condition.

Remark 2. Both Bézier conversion and subdivision make the sufficient condition less conservative.

Remark 3. As the number of the subdivision increases and each Bézier patch becomes smaller, the sufficient condition (minimal control point of the Jacobian B-spline be positive) approaches the necessary condition, (i.e. minimal Jacobian of the surface be positive).

Remark 4. The criterion is applicable to C^0 B-spline surfaces.

Based on above, we can develop the following optimization formulation, i.e. maximize the minimal Jacobian control point:

$$\max_{\boldsymbol{\gamma}} \min_{i,k} \overline{\widetilde{J}}^i{}_k(\boldsymbol{\gamma})$$

where

$i = 1$ to the total number of C^0 patches in $\mathbf{S}$;
$k = 1$ to the total number of control points of the Jacobian B-spline surface $J_{\overline{\widetilde{\mathbf{S}}}^i}$ of the B-spline patch $\overline{\widetilde{\mathbf{S}}}^i$;
$\boldsymbol{\gamma}$ represents all the internal control points in the surface $\mathbf{S}$.

The original min-max problem is hard to solve directly, it is thus reformulated as a bound formulation [25]

$$\begin{aligned} \max_{\boldsymbol{\gamma},\beta} \quad & \beta \\ \text{s.t.} \quad & \beta - \overline{\widetilde{J}^i}_k(\boldsymbol{\gamma}) \leq 0 \end{aligned} \tag{15}$$

Its formulation in the parameter space of the Coons surface (1) can be noted as

$$\begin{aligned} \max_{\boldsymbol{\gamma}^u,\beta} \quad & \beta \\ \text{s.t.} \quad & \beta - \overline{\widetilde{J}^i}_k(\boldsymbol{\gamma}^u) \leq 0 \\ & \gamma^u_j \in [0,1] \end{aligned} \tag{16}$$

The optimization terminates as soon as the objective function is larger than zero, i.e. a valid mesh is obtained. Our experience suggests that further iteration for an even larger minimal Jacobian does not necessarily lead to a better-quality mesh. Further, isogeometric analysis has been found to be robust against mesh distortion [26].

A gradient based optimizer (Method of Moving Asymptotes (MMA)) [27] is used to solve the above problem. Thus the gradient of the Jacobian control point $\overline{\widetilde{J}^i}_k(\boldsymbol{\gamma})$ over the design variables $\boldsymbol{\gamma}$ or $\overline{\widetilde{J}^i}_k(\boldsymbol{\gamma}^u)$ over the design variables $\boldsymbol{\gamma}^u$ are needed. From Eq. (13), we can see that

$$\begin{aligned} J'_{st} \quad = \quad & \sum_{\substack{i+k=s,\\ i\in[0,m-1],\\ k\in[0,m]}} \quad \sum_{\substack{j+l=t,\\ j\in[0,n],\\ l\in[0,n-1]}} mn \frac{\binom{m-1}{i}\binom{m}{k}}{\binom{2m-1}{i+k}} \frac{\binom{n}{j}\binom{n-1}{l}}{\binom{2n-1}{j+l}} \\ & \cdot(\Delta X'_{ij,u}\Delta Y_{kl,v} + \Delta X_{ij,u}\Delta Y'_{kl,v} - \Delta Y'_{ij,u}\Delta X_{kl,V} - \Delta Y_{ij,u}\Delta X'_{kl,v}) \end{aligned}$$

Here $\widetilde{J}'_{st}$ refers to the Jacobian B-spline surface's control points' sensitivities with respect to B-spline internal control points γ_j, i.e.$()' = ()/\partial\gamma_j$ where the B-spline internal control points can be constrained to, for example, stay within the bounding box of the original design domain. The sensitivities with respect to the transformed design variables γ^u becomes

$$\frac{\partial \widetilde{J}_k}{\partial \gamma^u_j} = \frac{\partial \widetilde{J}_k}{\partial \gamma_j}\frac{\partial \gamma_j}{\partial \gamma^u_j}$$

The latter part represents the Jacobian of the Coons surface and can be derived from (1).

Although both formulations (15) and (16) are valid for ensuring that the B-spline mesh is valid, the formulation (16) is used in this paper in order to ensure that control points' sensitivity over the design variables can be analytically calculated. Note that the control points are embedded in the parametric domain of the Coons patches (Eq. (5)). The initial positions for the internal control points during the optimization are from Eq. (5). The optimized positions $(\widetilde{u}^*_i, \widetilde{v}^*_j)$ are fed into Eq. (4) for sensitivity calculation in the shape optimization.

3.5 Results of mesh rectification

Three representative B-spline meshes with initially negative Jacobians and their respective corrected meshes are shown in Fig. 9, 10 and 11. All these meshes are quadratic B-spline meshes. The internal control points are shown in red. The process statistics in maximizing the minimal Jacobian for these three meshes is presented in Table 1, where N_{des} represents the number of design variables in the optimization, N_{cstr} represents the number of constraints, and N_I represents the number of optimization iterations. The subdivision time is $a \times b = 1 \times 1$. Among many examples that have been run, including these three meshes, the process converges usually within a few iterations, where the minimal Jacobian has changed from negative to positive. If the algorithm fails to converge within 10 iterations, the boundary has been found to be the cause of the problem, i.e. there is fold-over at the boundary itself where we intentionally create Coons patches with fold-over to test how well the approach works. Although not a theoretical proof, this suggests that the proposed mesh correction method is very effective and efficient in practice.

Table 1: Process statistics in maximizing Jacobian for B-spline meshes shown in figures 9, 10, and 11

Mesh	N_{des}	N_{cstr}	N_I	J_{min} (before)	J_{min} (after)
1	21	403	6	-0.006338	0.000144
2	21	403	3	-0.003968	0.000510
3	9	169	3	-0.002296	0.000018

4 Shape optimization examples

We apply the above developed B-spline mesh construction and nodal sensitivity computing approach in shape optimization of photonic crystals for maximizing band gaps. Shape optimization is in general used as a post-processing tool after topology optimization and we are likely to have very good starting guesses. A recent overview of topology optimization for nano-photonics is available in [28]. In this paper, the initial geometry of the shape optimization is modeled based on the geometric properties of optimal photonic crystals [29].

For lossless electromagnetic waves propagating in the xy plane, Transverse Magnetic (TM) ($\boldsymbol{E}$ field in the z direction) and Transverse electric (TE) ($\boldsymbol{H}$ field in the z direction) polarized waves can be described by two decoupled wave equations

$$\nabla^2 E_z(\mathbf{x}) + \frac{\omega^2 \varepsilon_r(\mathbf{x})}{c^2} E_z(\mathbf{x}) = 0, \qquad \text{TM},$$

$$\boldsymbol{\nabla} \cdot \left(\frac{1}{\varepsilon_r(\mathbf{x})} \boldsymbol{\nabla} H_s(\mathbf{x}) \right) + \frac{\omega^2}{c^2} H_z(\mathbf{x}) = 0, \qquad \text{TE}.$$

The distribution of dielectric is assumed periodic in the xy plane and constant in the z direction, i.e. $\varepsilon_r(\mathbf{x} + \boldsymbol{R}_j) = \varepsilon_r(\mathbf{x})$, where $\boldsymbol{R}_j$ are primitive lattice vectors with zero z component [29, 30]. The scalar fields satisfy the Floquet-Bloch wave conditions, $E_z = e^{i\boldsymbol{k}\cdot\mathbf{x}} E_{\boldsymbol{k}}$ and $H_z = e^{i\boldsymbol{k}\cdot\mathbf{x}} H_{\boldsymbol{k}}$, respectively, where $E_{\boldsymbol{k}}$ and $H_{\boldsymbol{k}}$ are cell periodic fields.

Combining either of the above TM and TE wave equations with the aforementioned periodic boundary conditions then leads to the following Hermitian eigenvalue problem

$$(\mathbf{K}_{\boldsymbol{k}} - \omega^2 \mathbf{M})\mathbf{h} = 0 \tag{17}$$

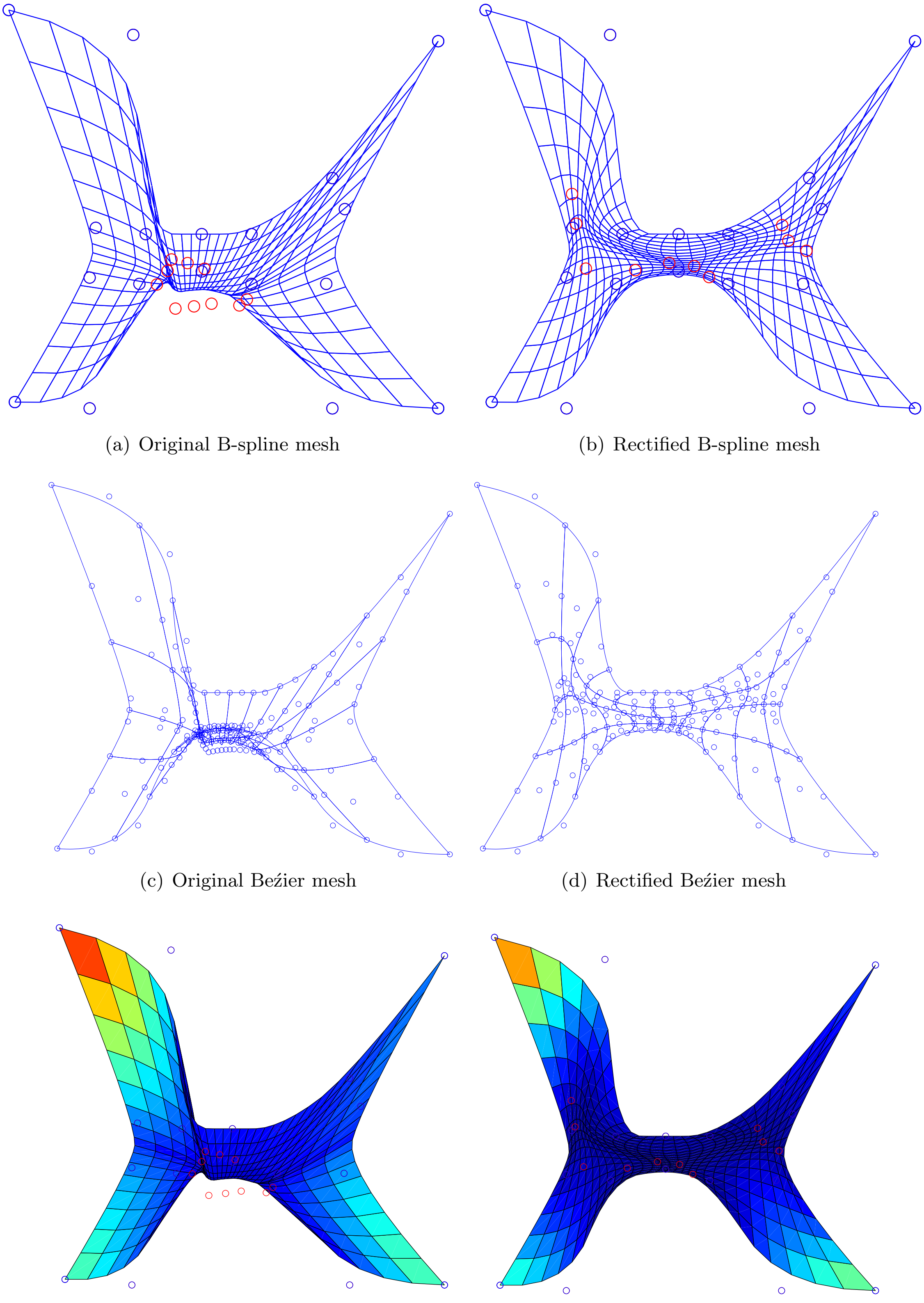

(a) Original B-spline mesh

(b) Rectified B-spline mesh

(c) Original Beźier mesh

(d) Rectified Beźier mesh

(e) Original Jacobian

(f) Rectified Jacobian

Figure 9: Mesh correction example 1. The bi-quadratic B-spline model consists of 7 × 4 control points.

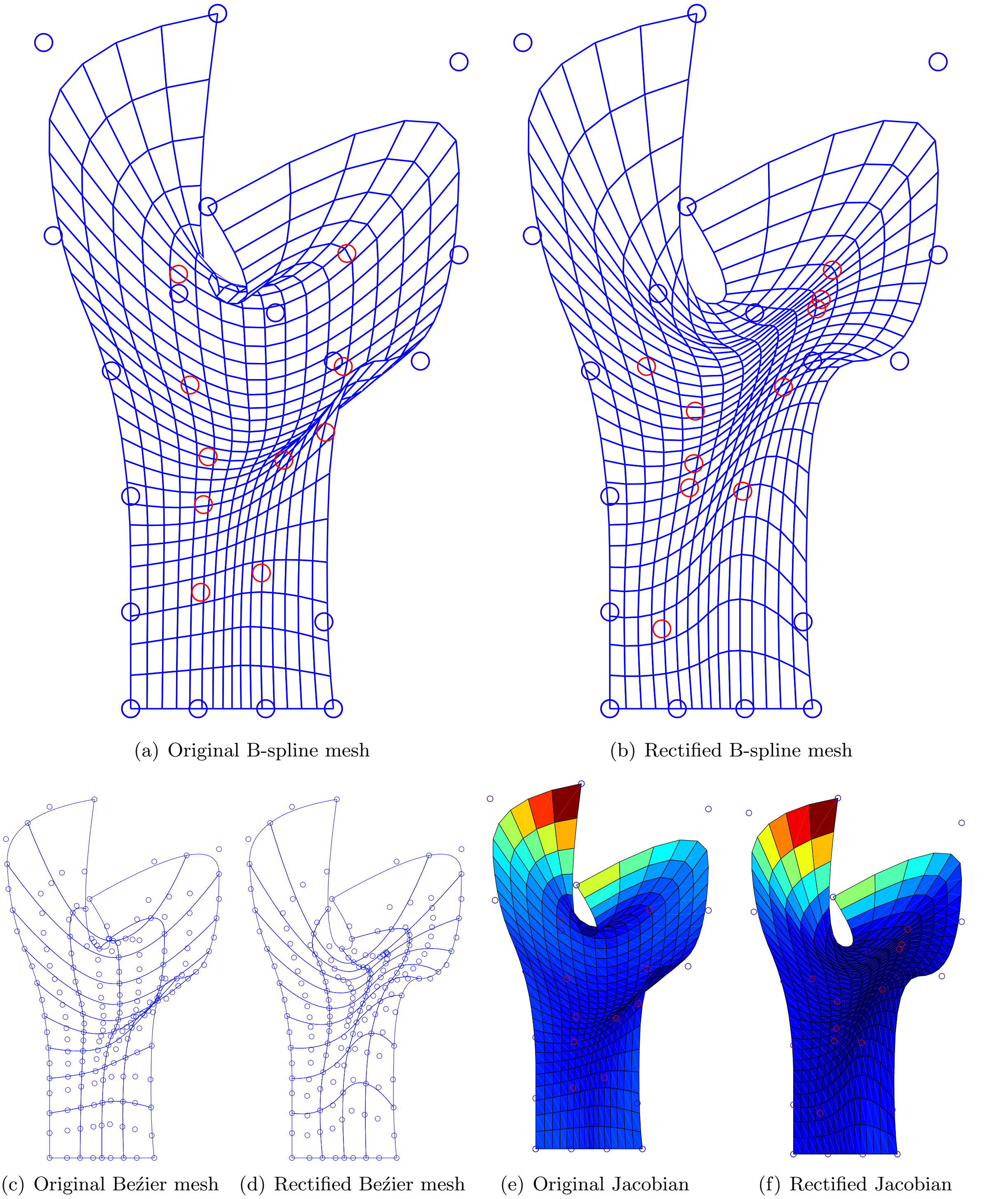

(a) Original B-spline mesh

(b) Rectified B-spline mesh

(c) Original Beźier mesh

(d) Rectified Beźier mesh

(e) Original Jacobian

(f) Rectified Jacobian

Figure 10: Mesh correction example 2. The bi-quadratic B-spline model consists of 4×7 control points.

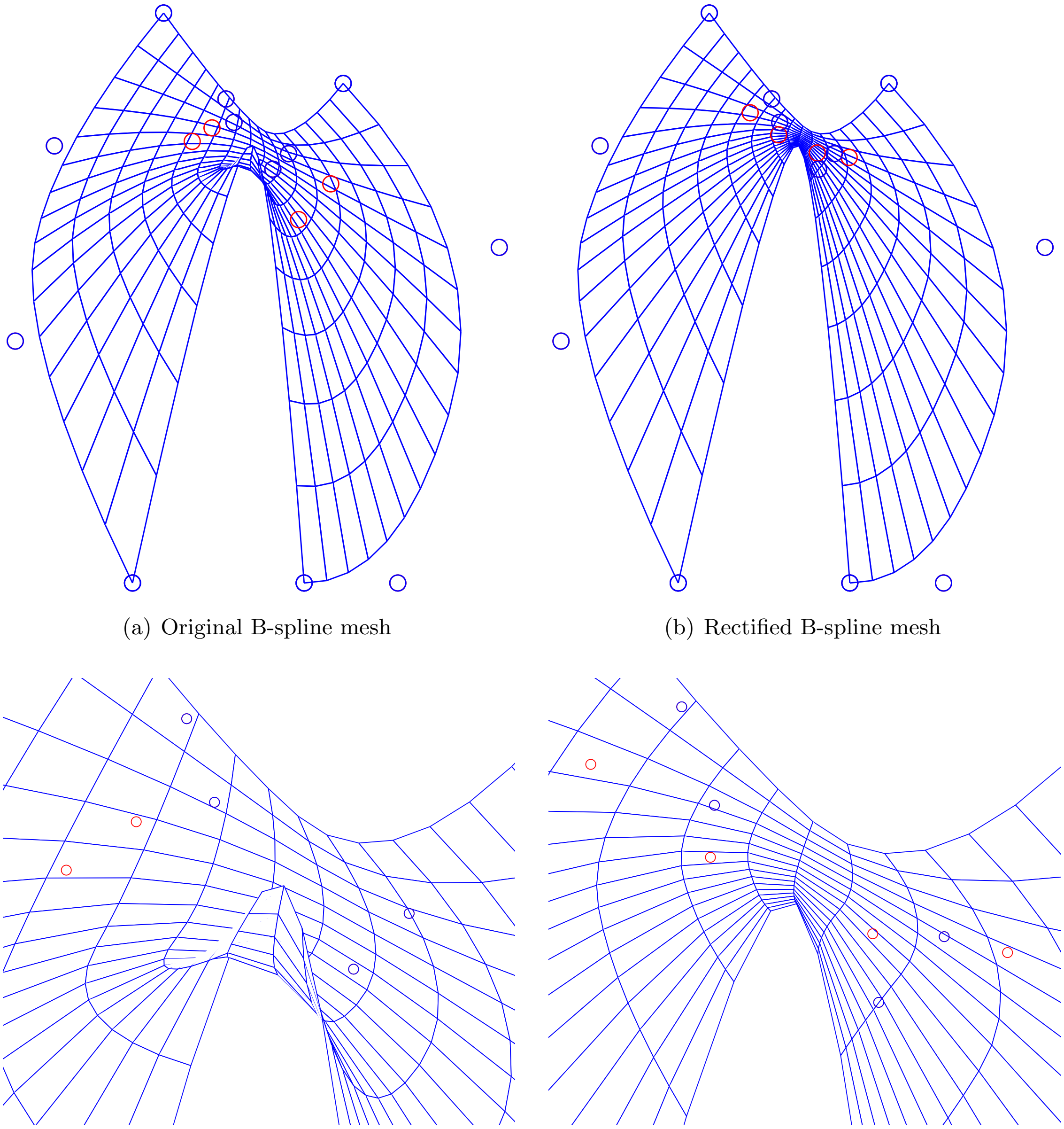

(a) Original B-spline mesh

(b) Rectified B-spline mesh

(c) Original mesh (magnified)

(d) Rectified mesh (magnified)

Figure 11: Mesh correction example 3. The bi-quadratic B-spline model consists of 4 × 4 control points.

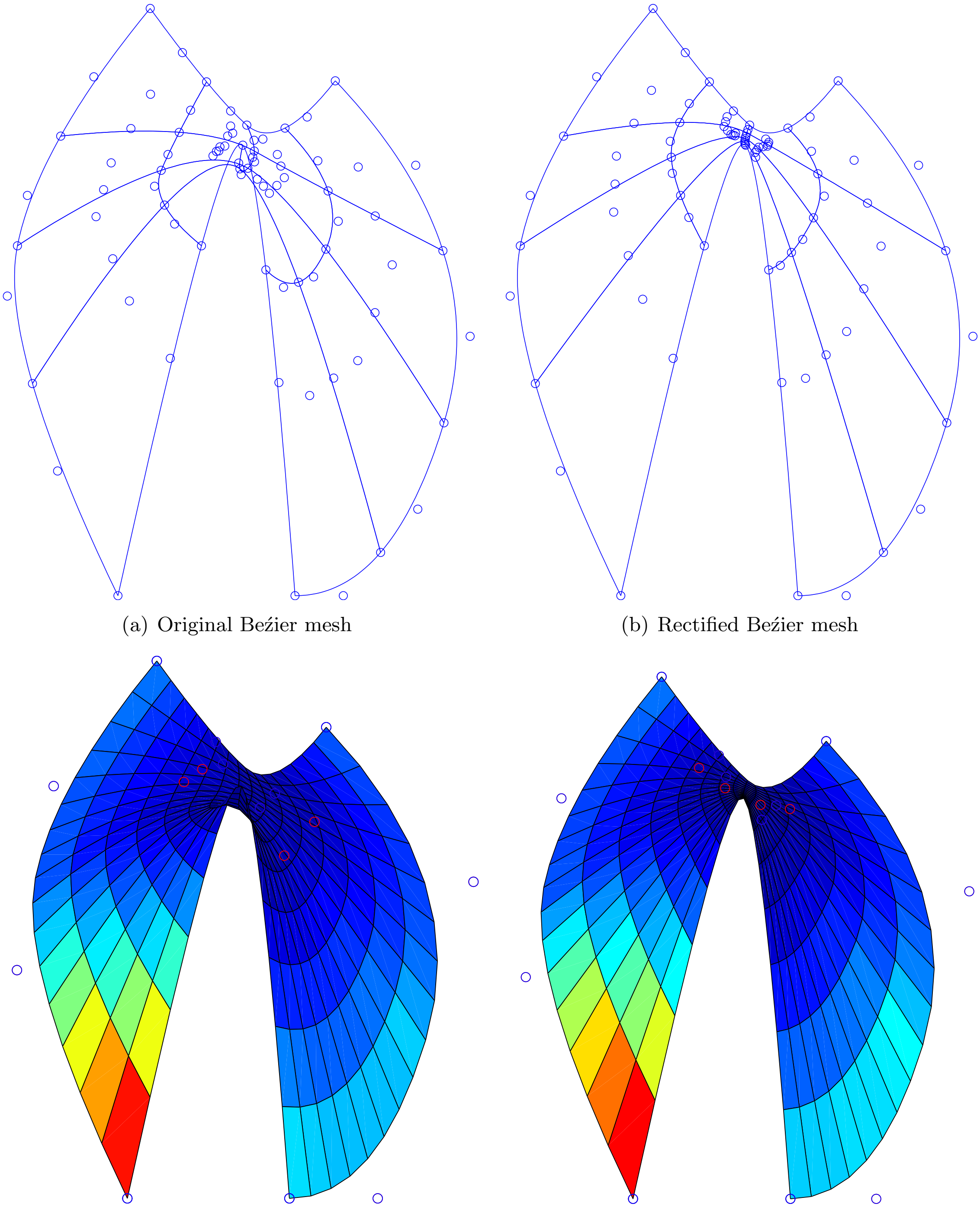

(a) Original Beźier mesh

(b) Rectified Beźier mesh

(c) Original Jacobian

(d) Rectified Jacobian

Figure 12: Mesh correction example 3. The bi-quadratic B-spline model consists of 4 × 4 control points.

where $\mathbf{K}_{\boldsymbol{k}}$ is the stiffness matrix for the wave vector $\boldsymbol{k}$ and $\mathbf{M}$ is the mass matrix. Solving (17) for wave numbers $\boldsymbol{k}$ belonging to the boundaries of the irreducible Brillouin zone we get a band diagram as shown in Fig. 15. We measure the relative band gap between bands n and $n+1$ as

$$\frac{\Delta w_n}{\omega_{c_n}} = 2\frac{\min_{\boldsymbol{k}} w_{n+1}(\boldsymbol{k}) - \max_{\boldsymbol{k}} \omega_n(\boldsymbol{k})}{\min_{\boldsymbol{k}} w_{n+1}(\boldsymbol{k}) + \max_{\boldsymbol{k}} \omega_n(\boldsymbol{k})} \tag{18}$$

where $\boldsymbol{k}$ are all wave vectors on the boundaries of the irreducible Brillouin zone.

Our goal here in shape optimization is to maximize the relative band gap $\Delta\omega/\omega_c$ (18). We use a gradient-based optimization. The sensitivities of a single modal eigenvalue are simply found as

$$\frac{\partial \lambda_i}{\partial \alpha_s} = \mathbf{h}_i^T \left[\frac{\partial \mathbf{K}}{\partial \alpha_s} - \lambda_i \frac{\partial \mathbf{M}}{\partial \alpha_s}\right] \mathbf{h}_i. \tag{19}$$

where $\lambda = \omega^2$ and the eigenvectors are normalized with respect to the kinetic energy, i.e. $\mathbf{h}_i^T\mathbf{M}\mathbf{h}_i = 1$. The sensitivity for eigen modes with multiplicity are found as [31, 32]. The sensitivities of the stiffness matrices and mass matrices with respect to the design variables can be directly traced to nodal (control point) sensitivities, as shown in [8]. Directly maximizing the relative band gap as shown in (18) is difficult. Instead, the problem is reformulated via a two-variable bound formulation

$$\begin{aligned}
\max_{\boldsymbol{\alpha},\beta_1,\beta_2} \quad & 2\frac{\beta_2 - \beta 1}{\beta_1 + \beta_2} \\
\text{s.t.} \quad & \omega_n(\boldsymbol{k}^i) - \beta_1 \leq 0,\ i = 1, \cdots, I \\
& \beta_2 - \omega_{n+1}(\boldsymbol{k}^i) \leq 0,\ i = 1, \cdots, I \\
& [\mathbf{K}(\boldsymbol{k}^i) - \omega^2\mathbf{M}]\mathbf{u} = 0,\ i = 1, \cdots, I \\
& \alpha_s^{\min} \leq \alpha \leq \alpha_s^{\max},\ s = 1, \cdots, N_{\text{des}}
\end{aligned}$$

where β_1 and β_2 are, respectively, the upper bound on the nth band and the lower bound on the $(n+1)$th band, $\boldsymbol{\alpha}$ are design variables, $\boldsymbol{k}^i$ represents the i-th wave vector in the irreducible Brillouin zone. It is solved as an ordinary non-linear programming problem by MMA.

Fig. 13 gives the overall flow chart of isogeometric shape optimization via Coons patches. For an input CAD geometry, Coons patches are first created. The internal control points for NURBS are then generated based on Eq. (5). A mesh validity check is invoked. If the minimum control point of the Jacobian of the NURBS patches is positive, a valid mesh is obtained. Otherwise, the mesh rectification procedure is invoked where the internal control point's parametric coordinates are optimized, as shown in Eq. (16) until the mesh is valid. The valid NURBS patches are then refined for isogeometric analysis. The sensitivity for the band gap and volume constraint over design variable (boundary curve's control points) α is then computed as shown in Eq. (19). The design variables for the shape are then optimized. A convergence check is done. If not converged, the Coons patches are then updated. The whole process repeats until a convergence criterion is met.

In the section below, we present several shape optimization examples. In the photonic crystal design (and in band gap design in general), it is accepted practice that optimization is done with respect to a subset of wave vectors (in Fig. 15 from Γ to X to M to Γ). A precondition for such practice is that the geometry has 45° symmetry. Since our goal here is to optimize the internal profile, in all examples in this section, only 1/8 of profiles corresponding to 45° symmetry are represented as design variables. The relative permitivity of the dielectric is $\varepsilon_r = 11.56$, corresponding to GaAs and that of air $\varepsilon_r = 1$.

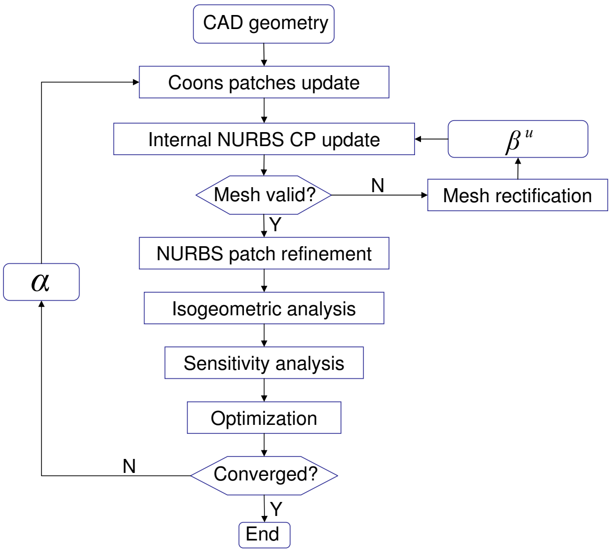

Figure 13: The flow chart of isogeometric shape optimization via Coons patches.

4.1 Bi-quadratic B-spline geometry for maximizing the first band gap for TE polarized waves

The goal of this design problem is to maximize the first band gap for TE polarized waves. The design is modeled with bi-quadratic B-spline geometries via Coons patches. It has 5 patches and 28 control points. The initial geometry is shown in Fig. 14.a. A 45-degree symmetry in geometry is imposed by constraining the control points with respect to the symmetric axes (shown as dotted lines in Fig. 14.a). The design boundary is the shape of the internal air inclusion and is defined by 4 quadratic B-spline curves each with 4 control points, shown in red. There are 4 linked nodes between the internal design boundary and the outer boundary, shown in magenta. (Note that linked nodes are control points of the Coons boundary that link the designed and/or fixed nodes. Their update during the optimization is based on their relative position with respect to their connected designed/fixed nodes in the initial design.) The analysis is done on the refined mesh. Two refined meshes have been used in the isogeometric analysis. The first one uses one refinement with 48 elements and 96 nodes. The second mesh uses refinement twice and has 192 elements 280 nodes. During the optimization, there are 5 design variables (two for controlling $\mathbf{P}_1$, one for controlling the diagonal movement of $\mathbf{P}_2$ and the other two for variable bounds β_1 and β_2 of the band gap) and 60 constraints (upper and lower bands for 30 sampled wave vectors along the Brillouin zone).

The criteria for terminating the optimization procedure is that the ratio of the objective function change per iteration over the initial objective function is smaller than 1.0e-7. The convergence history for both meshes are shown in Fig. 16. It takes 19 iterations for mesh 1 with the resulting relative band gap 29.34% and 18 iterations for mesh 2 with the relative band gap 29.07%.

The optimized geometry with one refinement and two refinements are, respectively, shown in Figs. 14.b and . 14.c. In the optimized geometry, the middle two control points for controlling the design boundary nearly overlap each other. The four corners in the optimized boundary are sharp. The optimized geometry from mesh 1 and mesh 2 are nearly identical. Fig. 14.d. shows the the

B-spline mesh and control points corresponding to the design in Fig. 14.c. Comparing Fig. 14.a and Fig. 14.d shows that the proposed B-spline construction via Coons patches is effective since it bypasses the specification of many interior B-spline control points. The profile of the optimized band gap from the second mesh is shown in Fig. 15.

The optimized geometries from meshes of two different element densities are nearly identical. It demonstrates, even with relatively fewer elements , isogeometric shape optimization still results in reasonably accurate optimized geometry.

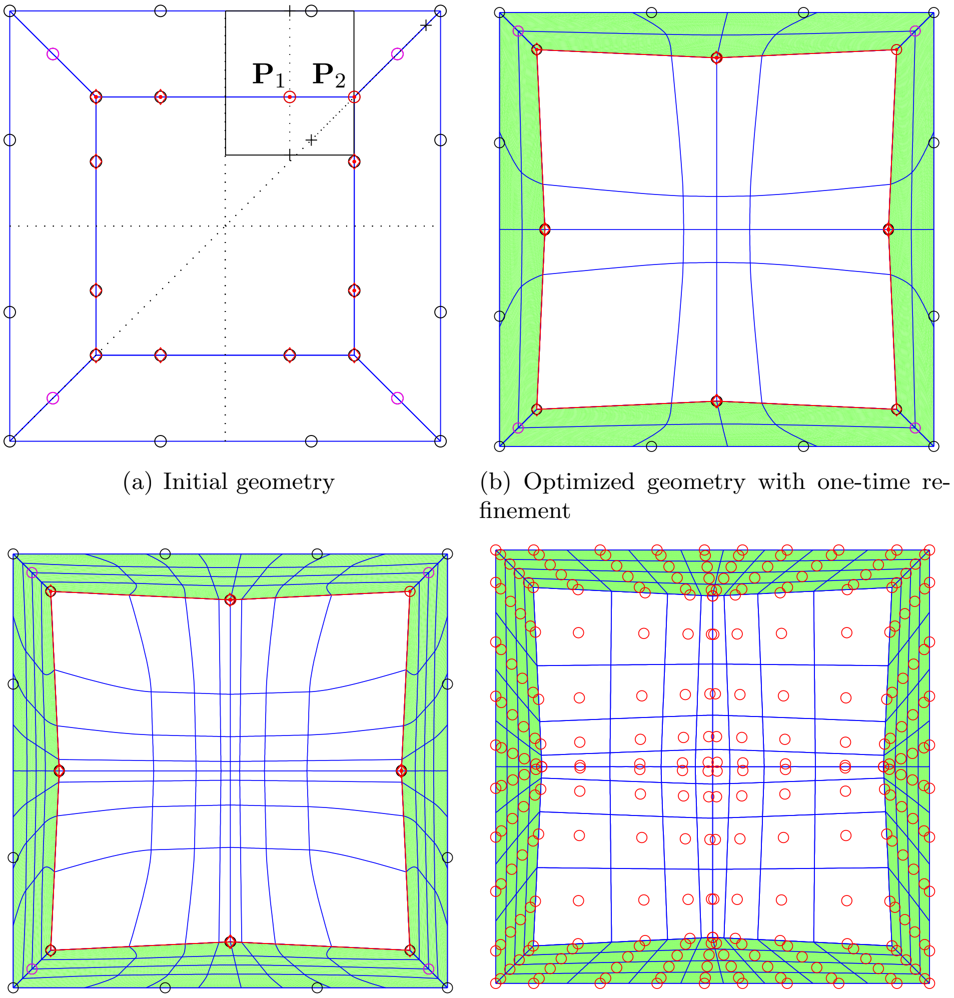

(a) Initial geometry

(b) Optimized geometry with one-time refinement

(c) Optimized geometry with two-time refinement

(d) Full NURBS model for the design in c)

Figure 14: Initial and optimized bi-quadratic geometry for maximizing band gap 1 for TE polarized light.

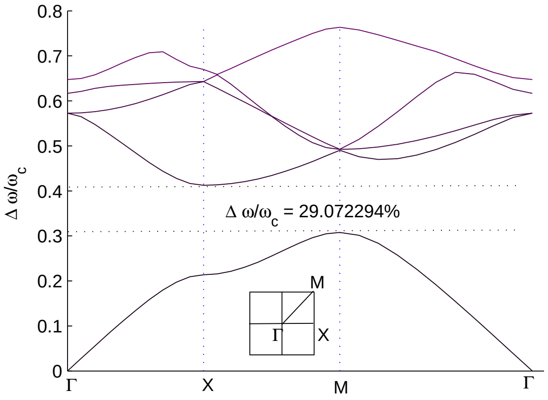

Figure 15: The band diagram from the optimized geometry in Fig. 14.c.

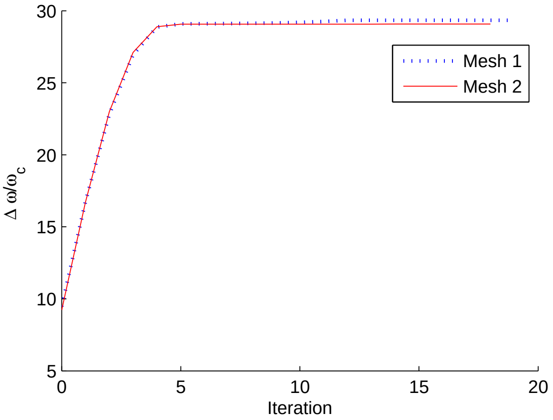

Figure 16: Convergence for the two optimizations in Fig. 14.

4.2 Bi-cubic NURBS geometry for maximizing the first band gap for the TE polarized light

The example above shows that the optimized geometry for maximizing the first band gap for TE polarized light exhibits sharp corners. For manufacturing reasons one may want to exclude sharp corners and small curvature radii. In order to allow curvature radii control to smooth out the sharp corners and to examine the trade-off between potential band gap loss and the imposed radius constraint, we use a bi-cubic NURBS geometry to model the design. Curvatures of the design boundary are controlled by constraining curvatures at sampled points on the boundary curves.

The initial design is shown in Fig. 17.a. There are 5 Coons patches and 56 nodes in the design model. The inner design boundary marked in red is defined by 4 cubic B-spline curves each with 7 control points (also in red). There are 8 linked nodes between the inner design boundary and the outer fixed boundary. The analysis model is refined once from the design model and there are total 128 bi-cubic elements and 281 nodes. The 45 degree symmetry is imposed for the design. Thus there are only 4 independent control points, $\mathbf{P}_1$, $\mathbf{P}_2$, $\mathbf{P}_3$ and $\mathbf{P}_4$. The corresponding allowed design ranges for the 4 points are shown in black in Fig. 17.a where two linear spans (one vertical for the middle point $\mathbf{P}_1$ and one along diagonal for the corner control point $\mathbf{P}_4$) and two box spans (for control points $\mathbf{P}_2$ and $\mathbf{P}_3$) are involved. All other control points for describing the design boundary are obtained through symmetry.

When no radius constraint is imposed, there are 8 independent design variables (6 for controlling the movement of 4 control points and and the other two as variable bounds for the band gap) and 60 constraints (upper and lower bands for 30 sampled wave vectors along the Brillouin zone). For radii constraints, an additional C^1 constraint is imposed, this leads to elimination of the corner control point $\mathbf{P}_4$ from being an independent variable. Thus, there are 7 independent design variables (5 for controlling control point movement and the other two as variable bounds for the band gap) and 100 constraints (60 for controlling band gaps and 40 for controlling curvatures for 20 sampled points on the 1/8 of the design boundary. Both positive and negative curvatures are constrained).

Fig. 17 shows the optimized shape under various radius constraints, including no radius constraint, and minimal radii ranging from 0.02, 0.05, 0.1, 0.25, to 0.4. When no radius constraint is imposed, the optimized shape has sharp corners, as shown in Fig. 17.b. When the minimal radius constraint is imposed, the corner becomes smoother. An example of the optimized shape with minimal radius 0.05 is shown in Fig. 17.c. (Note that in Figs. 17.b and 17.c., the 6 corner control points in the lower part of the design boundary are hidden for better display of the optimized boundary.) As the minimal radii increase further, the optimized shape approaches a circle, as shown in Fig. 17.d where the minimal radius is 0.4. Table 2 gives the relative band gap for the three designs.

Table 2: Relative band gap for three optimized designs

Minimum radii	r0	r0.05	r0.4
$\Delta\omega/\omega_c(\%)$	29.2039	29.1144	10.7297

As the minimum radii are increased to obtain a smoother corner to ensure the photonic crystal's manufacturability, the optimized band gap is reduced. The trade-off between the relative band gap and minimum radius constraint is plotted in Fig. 18 where more data pairs between the band gap and minimal radii are shown.

The maximum number of allowed iterations is 60. The number of iterations during the optimization with radius constraint 0, 0.02, 0.05, 0.1, 0.25, and 0.4 are respectively 60, 60, 40, 47, 34, and 28. Fig. 19 gives a representative example of convergence history where both the relative band gap and the radius over the iteration are plotted for optimization with the constraint of minimum radius 0.05. It shows that the radius constraint is active.

Fig. 20 shows the full NURBS model, including all control points and the isoparametric knot curves used in obtaining the optimized design with minimal radius 0.05.

This example demonstrates that the NURBS based shape parameterization allows fine control of the desired optimal shape. It also shows that the proposed NURBS construction via Coons patches is effective since it bypasses the specification of many interior NURBS control points.

4.3 Bi-quadratic NURBS geometry for maximizing the 8th band gap for TM polarized light

The goal of this design problem is to maximize the eighth band gap for TM polarized light. The design model is made of 24 Coons patches, consisting of 52 elements and 165 control points. With refinement once respectively in u and v direction, it leads to an analysis model consisting of 208 elements and 523 nodes. With two-time refinement, the analysis model consists of 832 elements and 1391 nodes. Fig. 22 shows the full NURBS analysis model (with two-time refinement) for the initial design A.

It has 18 design variables for controlling points from $\mathbf{P}_1$ until $\mathbf{P}_{10}$ and 65 constraints (60 for the upper and lower bands for 30 sampled wave vectors along the Brillouin zone and 5 for the convex constraints at $\mathbf{P}_1$, $\mathbf{P}_3$, $\mathbf{P}_5$, $\mathbf{P}_7$, and $\mathbf{P}_9$). Note that the points $\mathbf{P}_1$ and $\mathbf{P}_5$ are limited to horizontal movements and $\mathbf{P}_6$ and $\mathbf{P}_{10}$ are limited to diagonal movements. All other points are allowed to move in both x and y directions.

Fig. 21 shows the two initial designs and the optimized designs with one-time mesh refinement and two-time mesh refinement. The allowable design variable ranges are shown in Figs. 21.a and 21.b. Figs. 21.c and 21.d show the design from mesh with one-time refinement after 50 iterations. Figs. 21.e and 21.f show the nearly identical optimized design from a mesh with two-time refinement with the initial designs respectively from Figs. 21.c and 21.d. It shows how initial designs from two different geometry converge to nearly identical optimized shapes.

The optimization converges smoothly. An example of the convergence history for design A in Fig. 21, is shown in Fig. 24. The initial design for mesh 2 starts from the optimized geometry of mesh 1. The figure demonstrates that the optimized design (after 50 iterations) from the coarse mesh provides a good initial design for optimization with the refined mesh since there is no major change in the objective function during the optimization iteration for the mesh 2. Note that the denser mesh for the same geometry leads to slightly lower numerical values of the band gap. The relative band gap from Mesh 1, after 50 iterations is 43.26% and 43.00% from Mesh 2. Fig. 23 shows a mesh that does not have 45 degree symmetry, although the geometry does, the resulting band profiles remain nearly periodic where the considered wave vectors traverse the full quadrant of the Brillouin zone, from Γ, X_1, M, Γ, X_2, M, and to Γ. Fig. 25 shows that the initial NURBS mesh generated automatically from the initial design (Fig. 21.a) was invalid. Note that the control point $\mathbf{P}_2$ lies to the left of line $\mathbf{L}$, thus leading to self-intersection. A magnified wireframe view of the invalid patch (containing points $\mathbf{P}_1$ and $\mathbf{P}_2$) in Fig. 21.a is shown in Fig. 21.c where the internal control points of the patch are shown in red. The wireframe view of the rectified mesh is shown in Fig. 21.d where the internal control points are varied to correct the mesh. The mesh correction only

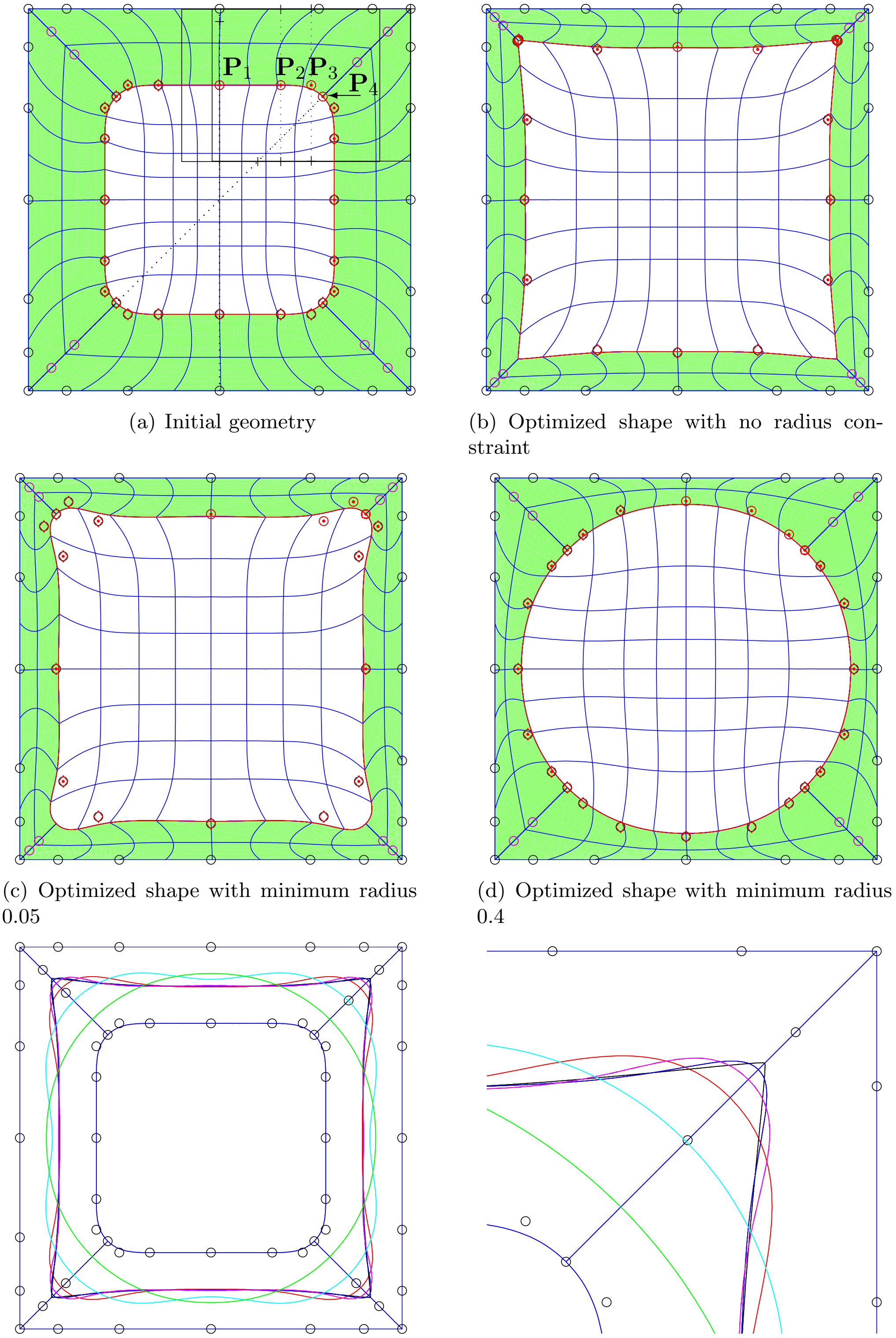

(a) Initial geometry

(b) Optimized shape with no radius constraint

(c) Optimized shape with minimum radius 0.05

(d) Optimized shape with minimum radius 0.4

(e) Initial and optimized shapes for minimal r0, r0.02, r0.05, r0.1, r0.25, r0.4

(f) Magnified view of (e)

Figure 17: Initial and optimized bi-cubic geometry under various minimal radii constraint. The objective is to maximize the 1st relative band gap for TE polarized light.

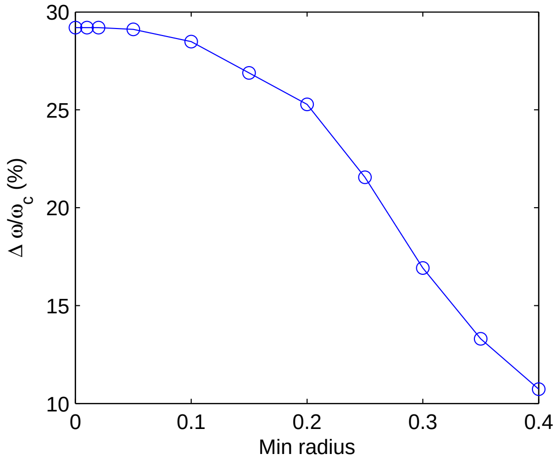

Figure 18: Trade off between relative band gap and minimum radius constraint.

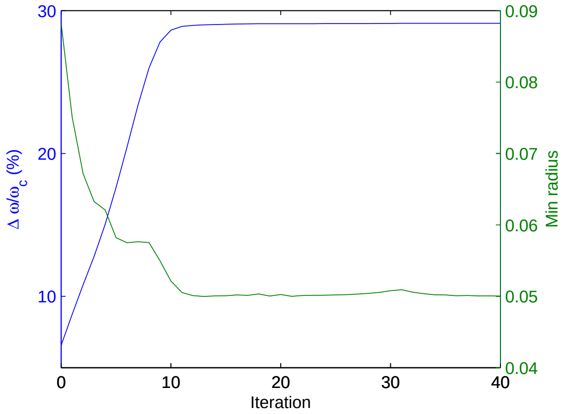

Figure 19: Convergence of band gap and radius constraint in optimization with minimal radius r0.005

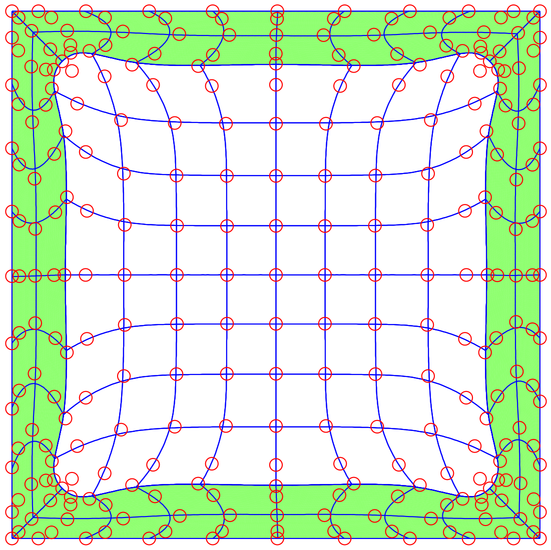

Figure 20: The full NURBS model of the optimized design under minimal radius 0.05.

takes 2 iterations. The mesh rectification is only invoked once during the optimization iteration.

5 Conclusions

This paper presents an approach that allows isogeometric optimization of topologically complex geometries. The approach is based on using multiple Coons patches to model design geometry, and using exact boundary conversion of Coons patches to NURBS patches to obtain the analysis model, and augmenting it with a built-in mesh rectifier to ensure mesh injectivity.

We have successfully applied this approach in designing photonic crystals to maximize different band gaps. It demonstrates that the use of NURBS in shape parameterization allows fine control of desired shapes. The use of multiple compatible Coons patches has been found to be an effective way for optimizing topologically-complex geometries. More specifically,

- the use of Coons patches allows users to design boundary shapes without specifying internal control points of NURBS surfaces,
- the use of multiple patches allows topologically complex geometries to be represented as a collection of rectangular-like NURBS patches, and
- the embedding of NURBS internal control points in the parametric domain of the Coon patches allows the computing of analytical nodal sensitivities in gradient-based shape optimization.

In particular, the method of maximizing minimal control points of the Jacobian B-spline surfaces has been found to be very useful in ensuring that the B-spline meshes generated from the Coons patches are valid.

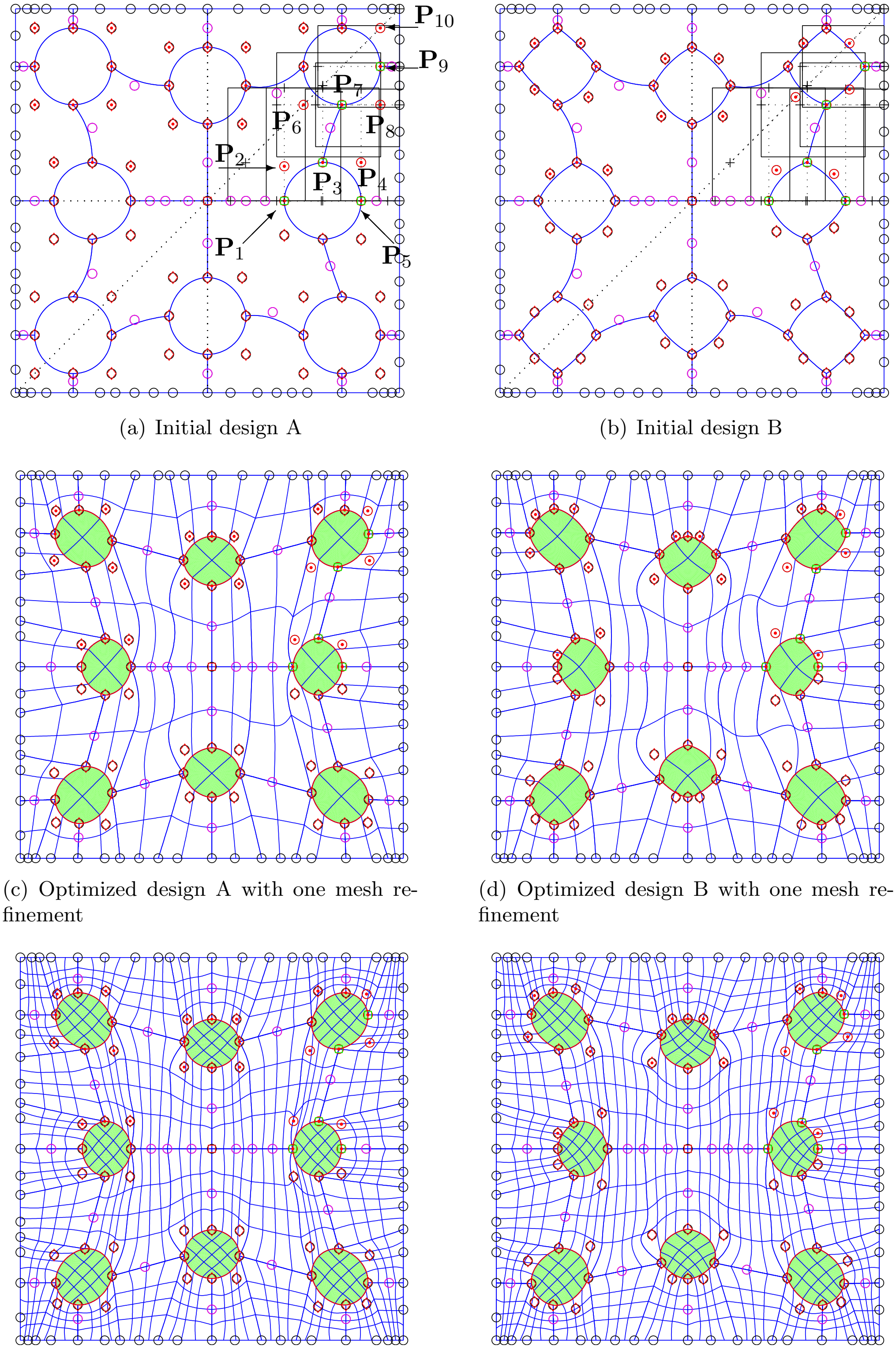

(a) Initial design A

(b) Initial design B

(c) Optimized design A with one mesh refinement

(d) Optimized design B with one mesh refinement

(e) Optimized design A with two mesh refinement

(f) Optimized design B with two mesh refinements

Figure 21: Two initial designs and the optimized designs for maximizing band gap 8 for TM polarized light.

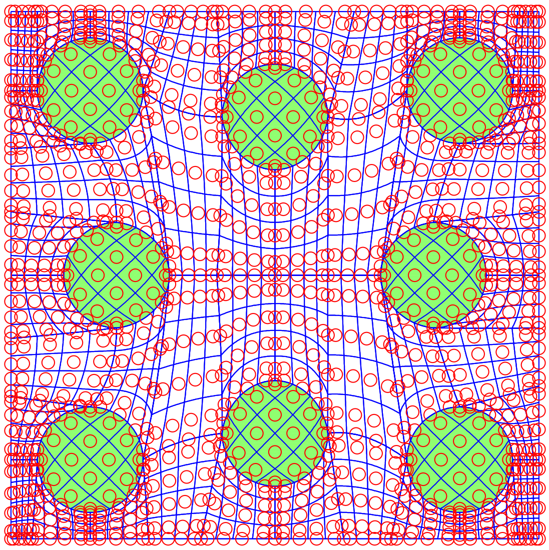

Figure 22: The full NURBS analysis model of the initial design A: red points are control points and blue curves are isoparametric knot curves.

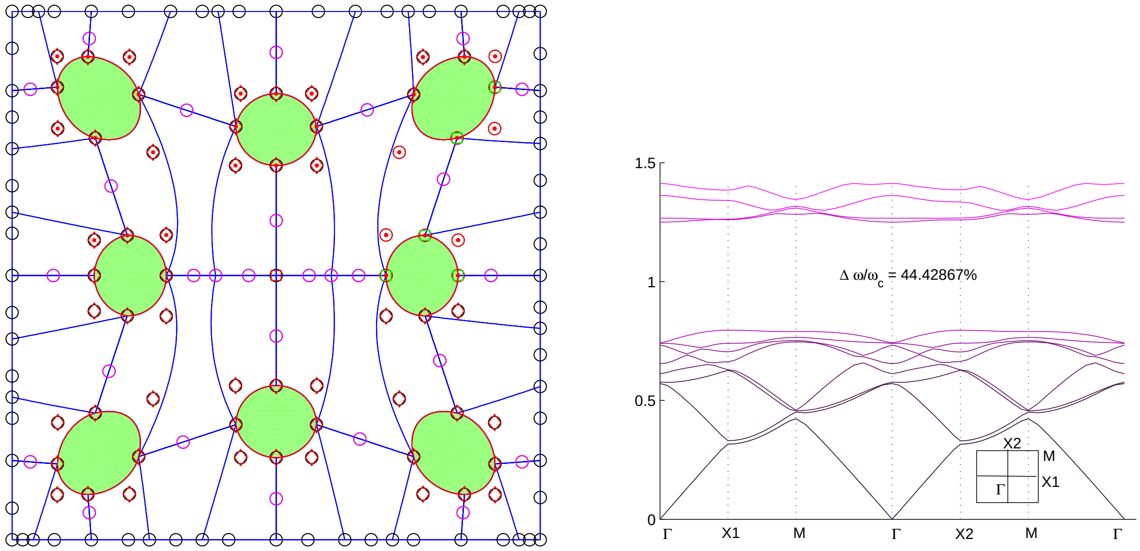

(a) Asymmetric mesh

(b) Band gap profile

Figure 23: Band gap profiles for the 45 degree symmetric geometry where the mesh does not have such a symmetry. The band gap is obtained by considering wave vectors of a quadrant of the zone, traversing from point Γ, X_1, M, Γ, X_2, M, and to Γ.

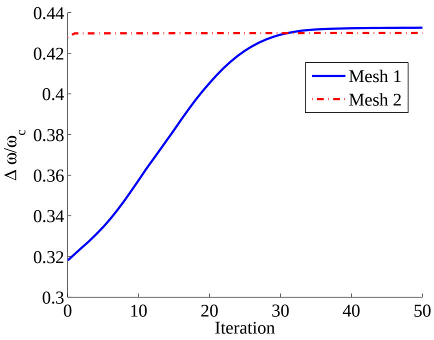

Figure 24: Convergence in optimization with mesh 1 and mesh 2 for maximizing the 8th band gap for the TM polarized light.

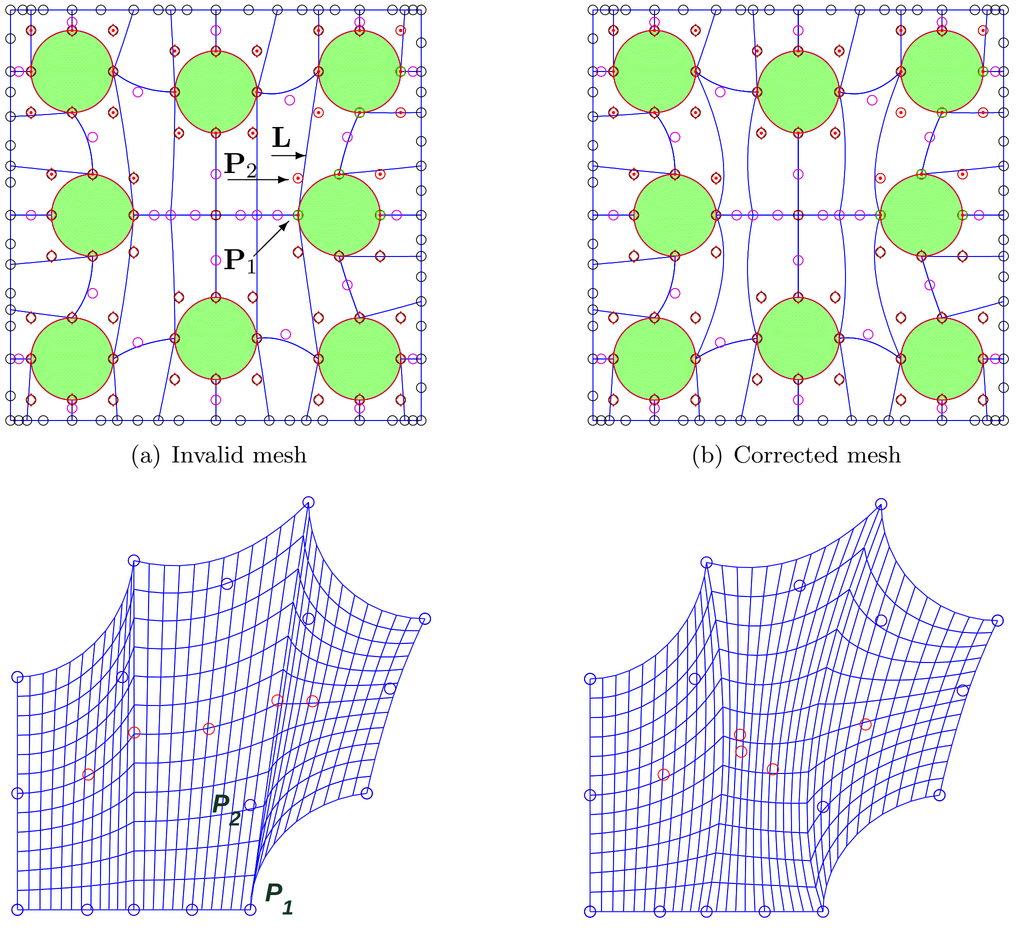

(a) Invalid mesh

(b) Corrected mesh

(c) Magnified wireframe view of invalid patch in a)

(d) Magnified wireframe view of corrected patch in b)

Figure 25: B-spline mesh rectification by moving internal control points.

Our future work would extend this approach to 3D structures. One of the advantages of our approach to isogeometric shape optimization is that it can bypass the specification of internal control points. Of course, when 3D shell structures are concerned, the internal points are part of independent design variables, thus this advantage does not apply. However, our approach might still be useful in that the Coons patch might provide a base for generating good initial internal control points for shape optimization. Further, our approach is naturally applicable to 3D solid structures where each Coons patch can be represented by 6 surfaces which provides a base for generating internal control points for B-spline solid.

References

[1] Braibant, V., and Fleury, C., 1984. "Shape optimal design using B-splines". *Computer Methods in Applied Mechanics and Engineering,* **44**, pp. 247 – 267.

[2] Samareh, J. A., 1999. *A Survey Of Shape Parameterization Techniques.* NASA Langley Technical Report.

[3] Hughes, T. J. R., Cottrell, J. A., and Bazilevs, Y., 2005. "Isogeometric analysis: CAD, finite elements, NURBS, exact geometry and mesh refinement ". *Computer Methods in Applied Mechanics and Engineering,* **194**, pp. 4135–4195.

[4] Yang, P., and Qian, X., 2007. "A B-spline based Approach to Heterogeneous Object Design and Analysis". *Computer-Aided Design,* **34**(2), pp. 95–111.

[5] Wall, W. A., Frenzel, M. A., and Cyron, C., 2008. "Isogeometric structural shape optimization". *Comput. Methods Appl. Mech. Engrg.,* **197**, pp. 2976 – 2988.

[6] Cho, S., and Ha, S. H., 2009. "Isogeometric shape design optimization: exact geometry and enhanced sensitivity". *Struct. Multidiscip. Optim.,* **38**, pp. 53 – 70.

[7] Nagy, A. P., Abdalla, M. M., and Gurdal, Z., 2010. "Isogeometric sizing and shape optimization of beam structures". *Computer Methods in Applied Mechanics and Engineering,* **199**, pp. 1216–1230.

[8] Qian, X., 2010. "Full analytical sensitivities in NURBS based isogeometric shape optimization". *Computer Methods in Applied Mechanics and Engineering,* **199**, pp. 2059 – 2071.

[9] Manh, N. D., Evgrafov, A., Gersborg, A. R., and Gravesen, J., To appear. "Isogeometric shape optimization of vibrating membranes". *Computer Methods in Applied Mechanics and Engineering.*

[10] Gravesen, J., Evgrafov, A., Gersborg, A. R., Manh, N. D., and Nielsen, P. N., 2010. "Isogeometric analysis and shape optimisation". In Proceedings of 23rd Nordic Seminar on Computational Mechanics, (A. Erikson and G. Tibert eds.), Stockholm 2010, pp. 14–17.

[11] Seo, Y., Kim, H., and Youn, S., 2010. "Shape optimization and its extension to topological design based on isogeometric analysis". *International Journal of Solids and Structures,* **47**(11-12), pp. 1618–1640.

[12] Seo, Y., Kim, H., and Youn, S., 2010. "Isogeometric topology optimization using trimmed spline surfaces". *Computer Methods in Applied Mechanics and Engineering.*

[13] Yablonovitch, E., 1987. "Inhibited spontaneous emission in solid-state physics and electronics". *Phys. Rev. Lett.,* **58**(20), May, pp. 2059–2062.

[14] John, S., 1987. "Strong localization of photons in certain disordered dielectric superlattices". *Phys. Rev. Lett.,* **58**(23), Jun, pp. 2486–2489.

[15] Christensen, P. W., and Klarbring, A., 2009. *An Introduction to Structural Optimization.* Springer.

[16] Haslinger, J., and Makinen, R. A. E., 2003. *Introduction to Shape Optimization: Theory, Approximation, and Computation.* SIAM, Philadelphia.

[17] Piegl, L., and Tiller, W., 1997. *The NURBS Book.* Springer-Verlag, New York.

[18] Cottrell, J., Hughes, T., and Reali, A., 2007. "Studies of refinement and continuity in isogeometric structural analysis". *Computer methods in applied mechanics and engineering,* **196**(41-44), pp. 4160–4183.

[19] Mørken, K., 1991. "Some identities for products and degree raising of splines". *Constructive Approximation,* **7**(1), pp. 195–208.

[20] Gain, J., and Dodgson, N., 2001. "Preventing self-intersection under free-form deformation". *IEEE Transactions on Visualization and Computer Graphics*, pp. 289–298.

[21] Lin, H., Tang, K., Joneja, A., and Bao, H., 2007. "Generating strictly non-self-overlapping structured quadrilateral grids". *Computer-Aided Design,* **39**(9), pp. 709–718.

[22] Hsu, W., Hughes, J., and Kaufman, H., 1992. "Direct manipulation of free-form deformations". In Proceedings of the 19th annual conference on Computer graphics and interactive techniques, ACM, pp. 177–184.

[23] Piegl, L., and Tiller, W., 1997. "Symbolic operators for NURBS". *Computer-Aided Design,* **29**(5), pp. 361–368.

[24] Farouki, R., and Rajan, V., 1988. "Algorithms for polynomials in Bernstein form". *Computer Aided Geometric Design,* **5**(1), pp. 1–26.

[25] Olhoff, N., 1989. "Multicriterion structural optimization via bound formulation and mathematical programming". *Structural and Multidisciplinary Optimization,* **1**(1), pp. 11–17.

[26] Lipton, S., Evans, J., Bazilevs, Y., Elguedj, T., and Hughes, T., 2010. "Robustness of isogeometric structural discretizations under severe mesh distortion". *Computer Methods in Applied Mechanics and Engineering,* **199**(5-8), pp. 357–373.

[27] Svanberg, K., 1987. "The method of moving asymptotes: A new method for structural optimization". *International Journal of Numerical Methods in Engineering,* **24**, pp. 359 – 373.

[28] Jensen, J. S., and Sigmund, O., 2011. "Topology optimization for nano-photonics - a review". *Laser & Photonics Reviews,* **5**, pp. 308 – 321.

[29] Sigmund, O., and Hougaard, K., 2008. "Geometric properties of optimal photonic crystals". *Physical Review Letters,* **100**(15), p. 153904.

[30] Joannopoulos, J., and Winn, J., 2008. *Photonic crystals: molding the flow of light.* Princeton Univ Pr.

[31] Jensen, J., and Pedersen, N., 2006. "On maximal eigenfrequency separation in two-material structures: the 1D and 2D scalar cases". *Journal of Sound and Vibration,* **289**(4-5), pp. 967–986.

[32] Seyranian, A., Lund, E., and Olhoff, N., 1994. “Multiple eigenvalues in structural optimization problems”. *Structural and Multidisciplinary Optimization,* **8**(4), pp. 207–227.